ISTANBUL TECHNICAL UNIVERSITY ★ GRADUATE SCHOOL OF SCIENCE ENGINEERING AND TECHNOLOGY

FABRICATION OF AMINO ACID FUNCTIONALIZED CNT/POLYAMIDE THIN FILM NANOCOMPOSITE DESALINATION MEMBRANES

M.Sc. THESIS

Aysa GÜVENSOY

Department of Chemical Engineering

Chemical Engineering Programme

DECEMBER 2018

ISTANBUL TECHNICAL UNIVERSITY ★ GRADUATE SCHOOL OF SCIENCE ENGINEERING AND TECHNOLOGY

FABRICATION OF AMINO ACID FUNCTIONALIZED CNT/POLYAMIDE THIN FILM NANOCOMPOSITE DESALINATION MEMBRANES

M.Sc. THESIS

Aysa GÜVENSOY
506161005

Department of Chemical Engineering

Chemical Engineering Programme

Thesis Advisor: Prof. Dr. Ş. Birgül TANTEKİN-ERSOLMAZ

DECEMBER 2018

ISTANBUL TEKNİK ÜNİVERSİTESİ ★ FEN BİLİMLERİ ENSTİTÜSÜ

AMİNO ASİT İLE FONKSİYONELLEŞTİRİLMİŞ KNT/POLİAMİD İNCE FİLM NANOKOMPOZİT DESALİNASYON MEMBRANI ÜRETİMİ

YÜKSEK LİSANS TEZİ

Aysa GÜVENSOY
506161005

Kimya Mühendisliği Anabilim Dalı

Kimya Mühendisliği Programı

Tez Danışmanı: Prof. Dr. Ş. Birgül TANTEKİN-ERSOLMAZ

ARALIK 2018

Aysa Güvensoy, a M.Sc. student of ITU Graduate School of Science Engineering and Technology with student ID 506161005, successfully defended the thesis entitled "FABRICATION OF AMINO ACID FUNCTIONALIZED CNT/POLYAMIDE THIN FILM NANOCOMPOSITE DESALINATION MEMBRANES", which she prepared after fulfilling the requirements specified in the associated legislations, before the jury whose signatures are below.

Thesis Advisor :	**Prof. Dr. Ş. Birgül TANTEKİN-ERSOLMAZ** İstanbul Technical University	.....
Jury Members :	**Prof. Dr. Ahmet SİRKECİOĞLU** İstanbul Technical University	.....
	Assoc. Prof. Dr. Zeynep ÇULFAZ-EMECEN Middle East Technical University	.....

Date of Submission : 16.11.2018
Date of Defense : 17.12.2018

ACKNOWLEDGEMENT

This work is partially supported by the Scientific and Technological Research Council of Turkey (TUBITAK) through the Grant No. 114Y165 and ITU - Scientific Research Projects through the Grant No. 40761.

First of all, I would like to express my sincere gratitude to my advisor Prof. Dr. Ş. Birgül Tantekin-Ersolmaz for her excellent guidance. She supported and encouraged me for pursuing my own ideas and planning my own independent research while I was still able to benefit from her profound knowledge and experience everytime I needed. I also like to thank her for teaching me what we learn during the process is as important as the results. I am proud to be her student.

I feel so lucky to be able to work with Dr. Sadiye Halitoğlu-Velioğlu and I am grateful to her for being my volunteer co-advisor. I would like to thank for her guidance, help and patience. She is one of the nicest people I have ever known and possibly the most meticulous researcher.

I would like to thank members of my research group, Süer Kürklüoğlu-Kocaoğlu and Cansu Yıldırım for their help and support. It is great to work with them. Besides being a very good company at the laboratory, Cansu greatly helped with my characterization studies. I am also grateful to Dr. Barış Yağcı from Koç University Surface Science and Technology Center for SEM, XPS and Raman analyses. I also would like to thank Prof. Dr. Ahmet Sirkecioğlu and Prof. Dr. Melek Tüter for allowing me to use some of their laboratory equipment.

Last but not least, I would like to thank my family. I am so lucky to have amazing parents like Ayşen and Sadık Güvensoy. They have always supported and motivated me to pursue my dreams and thaught me that the best investment a person can make is education. I am grateful to the newest member of my family, Uğurcan Morkoyun for being so supportive, motivating and optimistic during my entire university life. He contributed to every single page of this thesis and helped me to complete it just like he completes my life. Thank you!

November 2018

Aysa GÜVENSOY
Chemical Engineer

TABLE OF CONTENTS

Page

ABBREVIATIONS

TFC	**:** Thin Film Composite
TFN	**:** Thin Film Nanocomposite
CNT	**:** Carbon Nanotube
SWNT	**:** Single-Walled Carbon Nanotube
DWNT	**:** Double-Walled Carbon Nanotube
MWNT	**:** Multi-Walled Carbon Nanotube
IP	**:** Interfacial Polymerization
LMH	**:** Liters per square Meter per Hour
MF	**:** Microfiltration
UF	**:** Ultrafiltration
NF	**:** Nanofiltration
RO	**:** Reverse Osmosis
FO	**:** Forward Osmosis
PRO	**:** Pressure Retarded Osmosis
CVD	**:** Chemical Vapor Deposition
Asn	**:** Asparagine
ACA	**:** 8-Amino Caprylic Acid
TGA	**:** Thermal Gravimetric Analysis
DTG	**:** Differential Thermogravimetry
XPS	**:** X-Ray Photoelectron Spectroscopy
SEM	**:** Scanning Electron Microscope
FESEM	**:** Field Emission Scanning Electron Microscope
FTIR	**:** Fourier Transform Infrared Spectroscopy
AFM	**:** Atomic Force Microscopy
TEM	**:** Transmission Electron Microscope
PVDF	**:** Polyvinylidene Fluoride
DI	**:** De-ionized
Avg.	**:** Average
Std.	**:** Standart Deviation

SYMBOLS

J_i, J_j	: Water and salt flux
A, B	: Water and salt permeability constants
Δp	: Pressure difference across the membrane
$\Delta \pi$	: Osmotic pressure
c_{j_o}, c_{j_l}	: Salt concentrations in the feed and permeate sides of the membrane
w/v	: Weight to volume ratio
wt%	: Weight percent
V_p	: Permeate Volume
A	: Active membrane area
t	: Time
R	: Salt rejection
G_p	: Conductivity of permeate
G_f	: Conductivity of feed

LIST OF TABLES

Page

LIST OF FIGURES

Page

FABRICATION OF AMINO ACID FUNCTIONALIZED CNT/POLYAMIDE THIN FILM NANOCOMPOSITE DESALINATION MEMBRANES

SUMMARY

Water sustainability has become a worldwide concern due to limited natural resources and population growth. Considering that saline water constitutes nearly 97% of the total resources, water demand of agricultural, industrial and energy sectors leads a growing interest in desalination of seawater and brackish water. Reverse osmosis (RO) which constitutes approximately 65% of the worldwide desalination capacity has emerged as the leading technology for potable water production. Polyamide based thin film composite (TFC) membranes are extensively used in RO due to their superior separation performance; however, there are still important limitations such as permeability-selectivity trade-off, rejection of small and neutral species and susceptibility to fouling. Thin film nanocomposite (TFN) membranes has become a widely used approach to overcome limitations of conventional TFC membranes. These mixed matrix membranes are prepared by incorporation of various nanomaterials into the thin selective layer. Carbon nanotubes (CNTs) stand out as a potential TFN material due to their unique water transport properties. Experimental and computational studies suggest that functionalization of CNT tips may improve ion rejection as well.

In this study, effect of amino acid functionalized carbon nanotubes on the structure, morphology and separation performance of TFN membranes was investigated. Inspired by the structure of biological aquaporin channels, asparagine (Asn) amino acid was used as functional group in order to improve water permeability and salt rejection. The second amino acid, 8-aminocaprylic acid (ACA) was used due to its bulky structure in order to create steric hindrance for ions by narrowing the entrance of CNTs. Amino acid functionalization of carboxylated CNTs (COOH-CNTs) having average inner diameter of 1 nm was carried out via carbodiimide mediated reaction and confirmed by TGA, XPS and Raman spectrometry analyses. TFN membranes were prepared in two steps: First, functional CNTs dispersed in water by means of surfactant and centrifugated to remove large CNT bundles and impurities. Then CNT dispersion was vacuum-filtrated through the pores of support layer in order to provide partial aligment. Second, selective polyamide layer was synthesized via interfacial polymerization between MPD and TMC monomers. TFC membranes were also synthesized under identical conditions for comparison. Resulting TFC and TFN membranes were characterized by FTIR, XPS, SEM, AFM, polarized Raman spectrometry, water contact angle measurements and performance tests.

TFN membranes were prepared with COOH-CNT loadings of 2.4, 1.2, 0.6 and $0.3x10^{13}$ CNTs/cm^2 in order to determine optimum CNT loading. XPS, SEM, AFM and polarized Raman analyses showed that concentration of CNT significantly affects dispersion and alignment of CNTs inside the polymeric matrix as well as homogeneity, thickness and crosslinking ratio of polyamide layer. In addition, COOH-CNT incorporation decreased hydrophilicity of surface indicated by high water contact

angles for all loadings and surface roughness slightly increased as well. Based on salt rejection and water flux as well as structural and morphological properties, optimum CNT loading was determined to be $0.6x10^{13}$ CNTs/cm^2. Then, TFN membranes containing Asn-CNTs and ACA-CNTs were prepared at this loading and compared with TFC and TFN membranes contaning COOH-CNTs. Asn amino acid was thought to increase compatibility of CNTs with polyamide, leading formation of a thin, homogeneous and highly crosslinked polyamide layer having a similar surface with TFC. Asn also significantly increased surface hydrophicility compared to COOH due to its high hydrogen bonding capacity. Use of asparagine as functional group improved average water flux from 21.1 to 26.5 LMH and average salt rejection from 97.8% to 98.3% compared to TFC membranes. On the other hand, ACA amino acid resulted in a morphologically different polyamide layer, having pin-hole defects and reduced crosslinking ratio. Bulk structure of the molecule did not provide expected steric hindrance and caused a slight decrease in both water flux and salt rejection.

AMİNO ASİT İLE FONKSİYONELLEŞTİRİLMİŞ KNT/POLİAMID İNCE FİLM NANOKOMPOZİT DESALİNASYON MEMBRANI ÜRETİMİ

ÖZET

Sınırlı doğal kaynaklar ve hızlı nüfus artışı sebebiyle su yetersizliği dünya genelinde endişe verici bir hâl almıştır. Toplam su kaynaklarının %97'sinin tuzlu su olması, deniz suyu ve yeraltı suyundan desalinasyon ile içme ve kullanma suyu eldesine gösterilen ilginin giderek artmasına neden olmaktadır. Günümüzde desalinasyon, tarım, endüstri ve enerji sektörlerinin giderek artan su ihtiyacına bir çözüm olarak görülmeye başlanmıştır. Dünya genelindeki desalinasyon kapasitesinin %65'ini elinde tutan ters osmoz (TO), günümüzde içme ve kullanma suyu üretiminde lider bir teknoloji olarak görülmektedir. Poliamid temelli ince film kompozit (TFC) membranlar ise üstün ayırma özellikleri sebebiyle TO uygulamalarında yaygın şekilde kullanılmaktadır. Ticari TFC TO membranlarında istenen tuz giderimine ulaşılmasına rağmen, bu membranların performansını olumsuz etkileyen bazı problemler hâlâ çözüm beklemektedir. Bu problemlerden en önemlileri geçirgenlik-seçicilik dengesi, küçük ve nötr maddelerin giderimi ve kirlenmeye (fouling) yatkınlıktır. İnce film nanokompozit (TFN) membranlar, geleneksel TFC membranların performans sınırlarını aşmak amacıyla geliştirilmiş ve yaygınlaşmış bir yaklaşımdır. Bu karışık matrisli membranlar, çeşitli nanomalzemelerin ince seçici poliamid tabakasına katılmasıyla hazırlanmaktadır. Karbon nanotüp, grafen oksit, aquaporin ve zeolite umut vadeden nanomalzemeler arasındadır.

Karbon nanotüpler (KNT) üstün su geçirgenlik özellikleri sebebiyle potansiyel TFN malzemeleri arasında öne çıkmaktadır. KNT'lerin pürüzsüz ve hidrofobik duvarları, suyun hızlı bir şekilde geçmesine olanak tanımakta; ayrıca nanoboyutta bir kanalla kuşatılan su molekülleri arasındaki etkileşimler de su geçirgenliğinin artmasına katkıda bulunmaktadır. Deneysel ve hesaplamalı çalışmalar KNT uçlarının fonksiyonelleştirilmesi ile aynı zamanda iyon gideriminin de arttırılabileceğini öne sürmektedir. Bu çalışmada, amino asit ile fonksiyonelleştirilmiş KNT'lerin TFN membran yapısı, morfolojisi ve ayırma performansı üzerindeki etkileri incelenmiştir. Biyolojik hücre membranlarındaki aquaporin kanallarından esinlenilerek fonksiyonel grup olarak asparajin (Asn) amino asidi kullanılmış; bu sayede su akısı ve tuz gideriminin arttırılması hedeflenmiştir. Fonksiyonel grup olarak kullanılan ikinci amino asit olan 8-aminocaprylic acid (ACA), görece büyük moleküler yapısı sebebiyle, KNT uçlarını daraltarak sterik engel yaratmak ve tuz giderimini arttırmak amacıyla seçilmiştir.

Deneysel çalışmada kullanılan ortalama 1 nm iç çapa sahip tek duvarlı KNT'ler karboksilik asitle (COOH) fonksiyonelleştirilmiş olarak satın alınmıştır. Bu KNT'lere bağlı COOH'ların bir kısmının amino asitler ile yer değiştirmesi için EDC çapraz bağlayıcı kullanılarak COOH'lar aktifleştirilmiş ve amino asitlerin primer aminleriyle reaksiyona girmesi sağlanmıştır. Amino asit ile fonksiyonelleştirme TGA, XPS ve Raman spektrometre analizleriyle doğrulanmıştır. Asn ve ACA bağlı KNT'lerin TGA eğrilerinde, COOH bağlı KNT'lere göre yaklaşık 20°C daha yüksek sıcaklıkta

bozundukları gözlenmiştir. XPS analizinden elde edilen atomik bileşimlere göre, COOH-KNT'ler beklendiği gibi yalnızca karbon ve oksijen atomları içerirken; Asn ve ACA-KNT'lerin karbon ve oksijene ek olarak azot da içerdiği belirlenmiştir. XPS'ten elde edilen atomik yüzde dağılımları kullanılarak ve çapı 1.1 nm, kiralitesi (8,8) olan ideal bir KNT'den yola çıkılarak COOH'ların Asn'lere ve ACA'lara dönüşüm oranı sırasıyla %7.15 ve %9.72 olarak hesaplanmıştır. Raman analizi ise fonksiyonelleştirmenin KNT'lerin G/D oranında hafif bir düşüşe sebep olduğunu göstermektedir; fakat KNT stabiliteleri hâlâ kabul edilebilir seviyededir.

TFN membranların sentezi iki aşamadan oluşmaktadır: İlk olarak fonksiyonel KNT'ler yüzey etkinleştirici bir madde olan SDBS'nin yardımıyla suda dağıtılmakta, santrifüj edilerek büyük topaklardan ve safsızlıklardan arındırılmaktadır. Bu adımın eksikliği KNT'lerin kümelenerek poliamid ve destek membran arasında ikinci bir katman oluşturmasına ve tuz gideriminde ciddi bir düşüş yaşanmasına sebep olmaktadır. Mümkün olduğunca iyi dağıtılmış olan KNT'ler daha sonra vakum uygulanarak destek membran üzerine süzülür ve KNT'lerin destek membranın gözeneklerinde kısmen de olsa dik şekilde yönlenmesi sağlanır. İkinci adım ise gözeneklerine KNT'lerin yerleştirildiği destek membran yüzeyinin arayüzey polimerizasyonu ile ince seçici poliamid tabakası ile kaplanmasıdır. Su fazında monomer olarak MPD, organik fazda ise çözücü olarak hekzan, monomer olarak TMC kullanılmaktadır. Kullanılan destek membranın gözenek boyutu KNT demetlerinin yerleşmesine olanak verecek şekilde seçilmiş, monomer konsantrasyonları bu destek membrana göre optimize edilmiştir. Su fazında ayrıca KNT'lerin poliamid ile olan etkileşimini iyileştirmek amacıyla SDBS kullanılmaktadır. TFN membranlar ve karşılaştırma amacıyla birebir aynı koşullarda sentezlenen TFC membranlar FTIR, XPS, SEM, AFM, polarize Raman analizleri, su temas açısı ölçümleri ve performans testleri ile karakterize edilmiştir.

Optimum KNT yüklemesini belirlemek amacıyla dört farklı COOH-KNT konsantrasyonu ile (2.4, 1.2, 0.6 ve $0.3x10^{13}$ KNT/cm^2) TFN membranlar hazırlanmıştır. XPS analizinden elde edilen çapraz bağ oranları ile SEM ve AFM görüntüleri birlikte değerlendirildiğinde, KNT konsantrasyonunun KNT dağılımı ve yöneliminin yanı sıra poliamid tabakasının homojenliğini, kalınlığını ve çapraz bağ oranını önemli ölçüde etkilediği görülmüştür. $2.4x10^{13}$ KNT/cm^2 KNT yüklemesi ile hazırlanan TFN membranın TFC'den daha yüksek bir çapraz bağ oranına ve diğer TFN membranlara göre ince bir poliamid tabakasına sahip olduğu gözlenmiştir. Bu durum, yüksek konsantrasyonda KNT'lerin poliamid ile destek tabaka arasında üst üste birikerek üçüncü bir tabaka oluşturduğunu ve amaçlandığı gibi gözeneklere girerek dik şekilde yönelim sağlayamadığını düşündürmektedir. Daha düşük KNT konsantrasyonlarında ise KNT'lerin daha iyi dağılarak destek membranın gözeneklerine girdiği, gözeneklerin daralmasının sonucu olarak arayüzey polimerizasyonu sırasında MPD difüzyonunun sınırlandırıldığı ve poliamidin çapraz bağ oranının düşerek kalınlığının arttığı düşünülmektedir. $1.2x10^{13}$ KNT/cm^2 yükleme ile hazırlanan membranın çapraz bağ oranının ciddi şekilde düştüğü, poliamid yüzeyinin homojenliğinin bozulduğu gözlenmiştir. Daha düşük KNT yüklemelerinin, poliamid zincirlerinin çapraz bağlanması üzerinde olumsuz bir etki yaratmadığı; TFC'ye benzer yüzey şekillerine sahip oldukları gözlenmiştir. KNT yönelimini daha iyi değerlendirmek amacıyla polarize Raman spektrometrisine başvurulmuş; KNT'lerin dik ve yatay yönelimlerinin KNT yüklemesine bağlı olarak değişebileceği ve büyük ölçüde rastgele olduğu görülmüştür. AFM'den elde edilen yüzey pürüzlülüğü değerleri, pürüzlülüğünün KNT yüklemesi ile doğrudan ilişkili olmadığını fakat genel olarak KNT katkısı ile birlikte TFC'ye göre daha yüksek bir

pürüzlülük gözlendiğini göstermektedir. Ayrıca su temas açısı ölçümlerine göre KNT katkısının yüzey hidrofilikliğini ciddi biçimde düşürdüğü belirlenmiştir. Bu da KNT'lerin hidrofobik duvarlarının yüzeye ve yüzeye yakın bölgelere etki ettiğini göstermektedir. Su akısı ve tuz giderimi değerleri incelendiğinde, 2.4 ve $1.2x10^{13}$ KNT/cm^2 yüklemeleri ile hazırlanan membranların tekrarlanabilirliğinin düşük olduğu ve poliamid tabakasındaki deformasyonlar sebebiyle tuz giderimlerinin %93'lere kadar düştüğü görülmektedir. $0.3x10^{13}$ KNT/cm^2 KNT yüklemesi TFC membranların ortalama tuz giderimini korurken ortalama su akısında belirgin bir düşüşe sebep olmuştur. Öte yandan $0.6x10^{13}$ KNT/cm^2 KNT yüklemesi ile hazırlanan TFN membranlar TFC'ler ile kıyaslandığında ortalama tuz gideriminin %97.8'den %98.3'e; ortalama su akısının ise 21 LMH'tan 24 LMH'a yükseldiği görülmüştür. Yapısal ve morfolojik karakterizasyonlar ile performans değerleri birlikte değerlendirildiğinde $0.6x10^{13}$ KNT/cm^2 optimum KNT yüklemesi olarak belirlenmiştir.

Belirlenen bu optimum KNT yüklemesinde Asn ve ACA ile fonksiyonelleştirilmiş olan KNT'ler kullanılarak TFN membranlar hazırlanmış ve hem COOH-KNT içeren TFN membranlar ile hem de TFC membranlar ile kıyaslanmıştır. TFC'ye benzer şekilde homojen, ince ve çapraz bağ oranı yüksek bir poliamid tabakasının sentezlenmesine imkan vermesi sebebiyle Asparajin amino asidinin KNT'ler ile poliamid arasındaki etkileşimleri iyileştirdiği düşünülmektedir. Ayrıca Asn, yüksek hidrojen bağı kurma kapasitesine bağlı olarak yüzey hidrofilikliğini önemli ölçüde arttırmış; KNT duvarlarının hidrofobik etkisini dengeleyerek yüzey hidrofilikliğini TFC membranların seviyesine yükseltmiştir. Asn amino asidinin fonksiyonel grup olarak kullanılması TFC'ye kıyasla ortalama saf su akısını 21 LMH'tan 26.5 LMH'a, ortalama tuz giderimini ise %97.8'den %98.3'e yükseltmiştir.

ACA amino asidi ise morfolojik olarak diğer TFC ve TFN membranlardan daha farklı bir poliamid tabakası oluşmasına sebep olmuştur. Bu molekülün göreceli büyük yapısı ve moleküler etkileşimleri sebebiyle arayüzey polimerizasyonu sırasında poliamid zincirlerinin çapraz bağlanmasına engel olduğu; daha lineer ve kalın bir poliamid sentezlenmesine; ayrıca poliamid yüzeyinde halkasal yapılar olarak kendini belli eden bazı deformasyonların oluşmasına sebep olduğu düşünülmektedir. Molekülün büyüklüğü, beklendiği gibi sterik engel yaratarak KNT ağzının daraltılmasına ve tuz giderimin artmasına sebep olmamış; tersine hem tuz giderimini hem de su akısını düşürmüştür.

1. INTRODUCTION

Water sustainability has become a worldwide concern due to limited natural resources and population growth. While global water demand has been raised by approximately 1% per year for the last decade; factors such as climate change, urbanization, de-forestation and insufficient wastewater treatment have made fresh water availability even more challenging [1, 2]. Considering that saline water constitutes nearly 97% of the total resources, water demand of agricultural, industrial and energy sectors leads a growing interest in desalination of seawater and brackish water [3].

Reverse osmosis (RO) which is a membrane-based separation process stands out as the dominant desalination technology [4]. Polyamide based thin film composite (TFC) membranes, prepared by interfacial polymerization technique, are extensively used in seawater reverse osmosis (SWRO) applications due to their superior separation performance and stability; however, important limitations, such as permeability-selectivity trade-off, rejection of small and neutral species, and susceptibility to fouling, still exist [5]. Nanomaterial incorporation has become a widely used approach to overcome these limitations of conventional TFC membranes. Thin film nanocomposite (TFN) membranes are synthesized by embedding different nano-size materials into the polyamide layer of the TFC membranes. Novel materials such as carbon nanotubes, nanoporous graphene, graphene oxide, metal oxides, metals and aquaporin proteins are considered promising [6, 7]. Among these nanomaterials, carbon nanotubes (CNT) and aquaporins stand out due to their unique water permeability properties [8]. Consisting of condensed carbon rings arranged in a cylindrical shape, carbon nanotubes have highly smooth and hydrophobic walls which greatly reduce the friction; and rearrengement of water molecules confined in CNT nanospace also contributes to fast water transport [8, 9]. Furthermore, functionalization of CNTs enables the introduction of various chemical interactions and gate-keeper controlled chemical separation mechanisms [8]. On the other hand, aquaporins are natural water channel proteins which are ubiquitously found in the

biological cell membranes [10]. Their remarkable water permeability and ion rejection properties have inspired design of biomimetic membranes [11].

The main goal of this thesis is to investigate the effect of amino acid functionalized CNTs on the structure, morphology and separation performance of TFN membranes. For this purpose, two different amino acid structures have been chosen. Inspired by the structure of biological aquaporin channels, asparagine (Asn) amino acid will be used as a functional group in order to improve water permeability and salt rejection. The second amino acid, 8-aminocaprylic acid (ACA), is chosen due to its bulky structure in order to create steric hindrance for ions by narrowing the entrance of CNTs. Hence, it is foreseen that the salt rejection capacity of the membrane would be increased. With this intention, first optimum CNT loading of TFN membranes will be determined for the specific synthesis conditions of interfacial polymerization. Then, TFN membranes will be prepared using amino acid functionalized CNTs at the optimum loading. Finally, structure, morphology and separation performance of TFN membranes will be characterized and compared with each other as well as that of TFC membranes.

The organization of the thesis is as follows: The theoretical background for reverse osmosis, TFC and TFN membranes, CNTs and functional groups are presented in Chapter II. Materials and methods used in the experimental study are described in Chapter III. Results are presented and discussed in Chapter IV, and Chapter V contains conclusions and recommendations for the future work.

2. LITERATURE REVIEW

2.1 Reverse Osmosis Technology

Reverse osmosis (RO) which constitutes approximately 65% of the worldwide desalination capacity has emerged as the leading potable water production technology today [4]. Reverse osmosis can be defined as a pressure-driven membrane separation process. A reverse osmosis membrane is highly permeable to water while effectively limiting the passage of solutes e.g. salt ions. In osmosis phenomena, osmotic pressure difference between the high and low salt concentration sides of the membrane induces spontaneous passage of water molecules along its own concentration gradient as shown in Figure 2.1. In reverse osmosis, a pressure difference which is higher than the osmotic pressure is applied so that water begins to flow in the opposite direction by overcoming its concentration gradient. The water flux, J_i, depends on the water permeability constant A, pressure difference across the membrane Δp, and osmotic pressure differential $\Delta \pi$, by the Equation 2.1 [12].

$$J_i = A(\Delta p - \Delta \pi) \tag{2.1}$$

Although water flux is closely related to the pressure difference across the membrane, flux of salt is theoretically independent of the pressure and can be described by Equation 2.2 in which C_j is the salt flux, B is the salt permeability coefficient, c_{j_o} and c_{j_i} are the salt concentration in the feed and permeate sides of the membrane, respectively [12].

$$J_j = B(c_{j_o} - c_{j_l}) \tag{2.2}$$

RO membranes have a pore size of 0.1-1 nm and fall into category of dense membranes in which transport of molecules takes place via solution-diffusion mechanism. For membrane materials having a pore size greater than 1-5 nm, permeate molecules can be transported by convective flow which applies to pore-flow model. Transport in microfiltration and ultrafiltration membranes is an example of pore-flow mechanism. If pore size is smaller than 1-5 nm as in RO membranes, permeate molecules should

be first dissolved in the membrane medium and then diffuse through this medium. Selectivity of the membrane relies on the differences in solubility and diffusivity of permeating species inside the membrane. While size exclusion is the dominant mechanism in terms of selectivity, molecular interactions between the membrane material and permeating species also contribute [12].

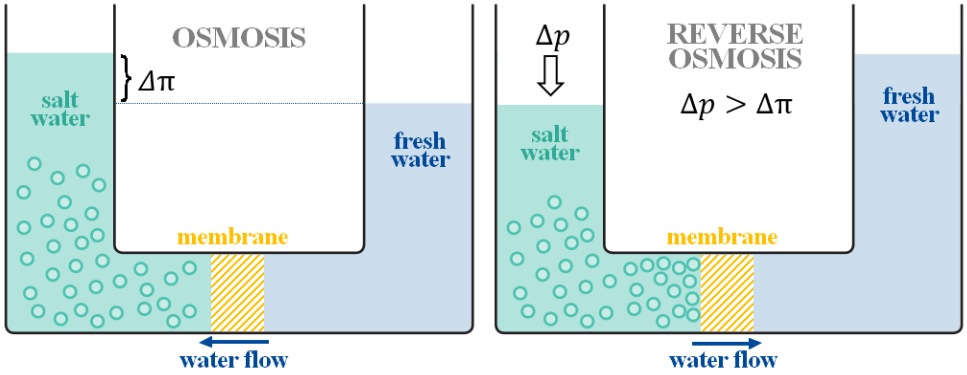

Figure 2.1: Schematic representations of osmosis and reverse osmosis.

History of modern reverse osmosis dates back to cellulose acetate films studied by Reid and Breton in 1959. They were able to fabricate cellulose acetate films having salt rejections around 98% and demonstrate utility of cellulose acetate films as RO membranes. However, their water fluxes were so low that reverse osmosis had not been considered as a practical process until first asymmetric cellulose acetate membranes were synthesized by Loeb and Sourirajan in 1962 [12]. Loeb-Sourirajan type membranes fabricated by phase inversion technique consisted of a dense skin layer and a porous substrate which allowed higher water fluxes, namely 10 times the flux of Reid and Breton's membranes, while retaining the same salt rejection. This discovery was recognized as a breakthrough and led to installation of few small RO plants in addition to launch of first commercial RO membranes [12-14]. Efforts to make thinner, more permeable and more selective membranes had continued and another breakthrough came in by the year 1972: Cadotte successfully carried out interfacial polymerization to synthesize a polyamide film on top of a porous support and fabricated the first thin film composite (TFC) membrane [14, 15]. TFC membranes have been widely used and remained as the "gold standard" in membrane industry to date [5].

2.2 Thin Film Composite (TFC) Membranes

Separation performance of TFC membranes have been considered as a remarkable improvement to asymmetric cellulose acetate membranes in terms of salt rejection and water flux. Another advantage is the stability over a pH range of 2 to 11 due to highly crosslinked aromatic structure of polyamide layer [5]. Support layer used for fabrication of TFC membranes is usually highly porous and made of polysulfone or polyethersulfone. This layer may be cast on a non-woven fabric such as polyester or polypropylene to increase mechanical strength. Selective polyamide layer is coated over support layer by in-situ interfacial polymerization reaction between two monomers dissolved in immiscible phases: m-phenylenediamine (MPD) or piperazine (PIP) dissolved in water and a triacyl chloride, usually trimesoyl chloride (TMC), dissolved in organic phase (e.g. hexane) [16, 17]. Also, additives such as trimethylamine (TEA), camphorsulfonic acid (CSA) or surfactants can be used. TEA is added as acid acceptor to neutralize the reaction medium while CSA is used for pH adjustment or protection of support integrity during heat curing. Surfactants such as sodium dodecyl sulfate (SDS) or sodium dodecyl benzene sulfonate (SDBS) are added to improve hydrophilicity and wettability of support layer [16].

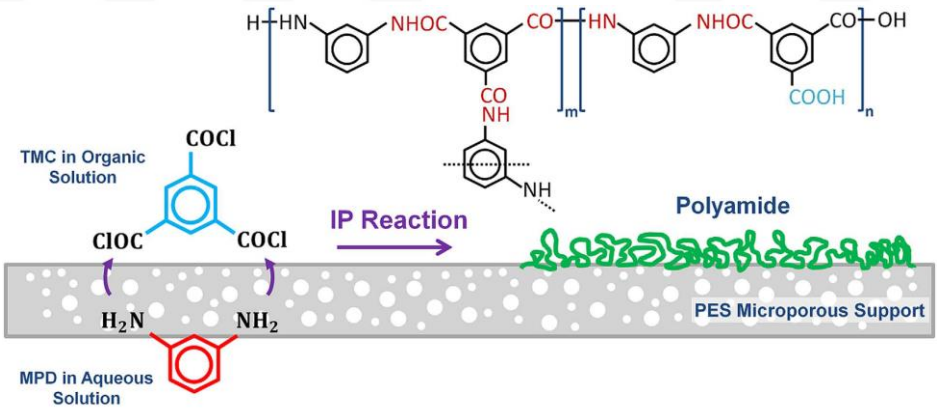

Figure 2.2: Interfacial polymerization between MPD and TMC monomers to form crosslinked and branched polyamide chains [19].

Although there are various recipes and procedures, usually the first step is to soak support layer in MPD solution. Then, excess MPD is removed and membrane is brought into contact with TMC solution. MPD starts to diffuse from water phase to water-organic interphase where it can react with TMC to form crosslinked or branched polyamide chains as shown in Figure 2.2. Reaction is self-limited due to growth of polyamide layer which shows mass transfer resistance against transport of MPD into

the reaction site. After reaction is completed, excess solvents are usually vaporized by heat curing [18].

2.2.1 Separation performance of TFC membranes

Separation performance of TFC membranes synthesized from MPD and TMC monomers has been repeatedly reported in the literature. However, salt rejection and water permeability of these laboratory-fabricated membranes may differ than those of commercial membranes as shown in Table 2.1. Differences may be originated from testing conditions such as transmembrane pressure or feed salinity as well as additives and surface modifications in commercial membranes which are not made public by manufacturers. Nonetheless, variability among literature reported data is evident even though same monomers and similar fabrication methods are used [18].

Table 2.1: Performance of selected laboratory-fabricated and commercial TFCs.

	Pressure (bar)	Feed salinity (ppm)	Salt rejection (%)	Water permeance ($L/(m^2 h)/bar$)
Yong et al. (2006) [20]	15.0	2000	98.0	2.00
Ghosh et al. (2008) [17]	15.5	2000	98.4	1.67
Kong et al. (2010) [21]	15.0	2000	97.5	0.76
Xie et al. (2012) [18]	15.5	2000	99.6	2.71
Chan et al. (2013) [22]	36.5	2500	97.6	0.32
Inukai et al. (2015) [23]	50.0	35000	97.0	0.54
Khorshidi et al. (2016) [19]	15.2	2000	98.8	0.70
DOW™ SW30HR-380 [24]	55.0	32000	99.7	0.53
Hydranautics™ SWC5-LD [25]	55.0	32000	99.8	0.69
TORAY™ TM840M-1760 [26]	55.0	32000	99.8	0.54

Manufacturer reported data is presented for commercial membranes.

2.2.2 Limitations of TFC membranes

As seen in Table 2.1, commercial TFC membranes have been remarkably improved in terms of salt rejection and they already meet the minimum salt concentration requirements specified for potable water. Increasing salt rejection may no longer be a hot research topic in the field of TFC membranes; however, there are still important

limitations to overcome such as permeability selectivity trade-off, poor rejection of small, neutral molecules and susceptibility to fouling.

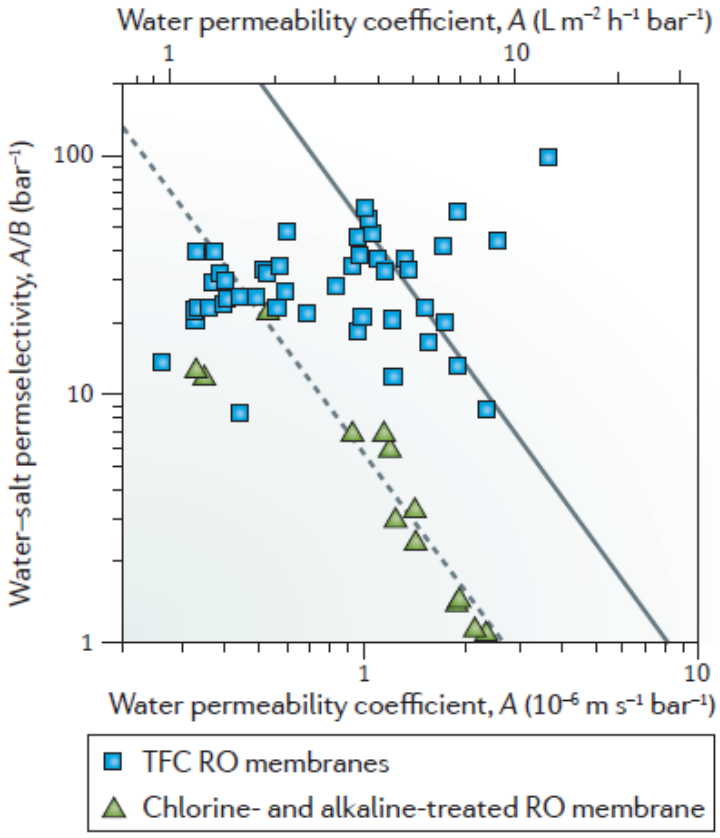

Figure 2.3: Perm-selectivity plot for commercial TFC RO membranes. Values represented by blue square are calculated from manufacturer specifications [9].

Permeability-selectivity trade-off is an intrinsic limitation for dense polymeric membranes in which water transport is governed by the solution-diffusion model as explained above. As the polyamide layer becomes fully cross-linked and denser to obtain high selectivity, it also increases the resistance against transport of water; thus, water flux drastically reduces. Analogous to Robeson plot, which is widely used for polymeric gas separation membranes, existence of an upper permeability-selectivity limit is suggested for RO membranes. As demonstrated in Figure 2.3, optimization of interfacially polymerized commercial RO membranes resulted in higher fluxes without compromising the salt rejection and moved the upper limit from dashed line to the solid line. However, an upper bound is still inevitable due to inherent characteristics of the polymeric material [5, 27].

Another difficulty with present membranes is the rejection of small and neutral species such as boron in seawater or toxic contaminants in wastewater (arsenic, fluoride,

endocrine disruptors). These species have adverse effects on human and crop health and their concentration should be decreased to acceptable levels strictly regulated by health organizations. Extensive post-treatment steps, such as further RO passes, ion exchange and oxidative chemical degradation are needed due to poor selectivity of present membranes [5, 27, 28].

Last but not the least important, fouling is a major problem for conventional TFC membranes. Organic fouling, scaling or bio-fouling can drastically reduce the separation performance of a polymeric membrane. Chemical cleaning procedures are unsustainable and they eventually shortens membrane life while increasing the energy consumption and operating costs [5]. There are surface modifications to increase antifouling property; however, this solution may be controversial since it often decreases the water permeability of the membrane by adding an extra resistance on top of the active layer.

2.3 Thin Film Nanocomposite (TFN) Membranes

Limitations of TFC membranes can be considered as the motivation behind development of thin film mixed matrix membranes. The term "thin film nanocomposite" (TFN) was first used by Hoek et al. in 2007 to describe their zeolite NaA dispersed polyamide RO membrane [29, 30]. Since then, nanomaterial incorporation has become a widely used approach to overcome limitations of conventional TFCs and the term "TFN" has settled into terminology. Novel materials such as carbon nanotubes, nanoporous graphene, graphene oxide, metal oxides, metals and aquaporin proteins are considered promising for TFN fabrication [6], [7].

2.3.1 Common nanocomposite membrane fabrication methods

Scope of the term "nanocomposite" is actually broader; several methods to fabricate nanocomposite membranes are depicted in Figure 2.4. Conventional nanocomposite membranes are usually prepared by dispersing nanomaterials into the dope solution prior to phase inversion and utilized for UF and MF applications. Nanocomposite substrate for TFC membranes can be prepared by similar methods and then coated with thin polyamide layer. This technique may be used to reduce water flux decline during the compaction of membrane or the internal concentration polarization taking place

inside the porous substrate especially in forward osmosis (FO) or pressure retarded osmosis (PRO) applications.

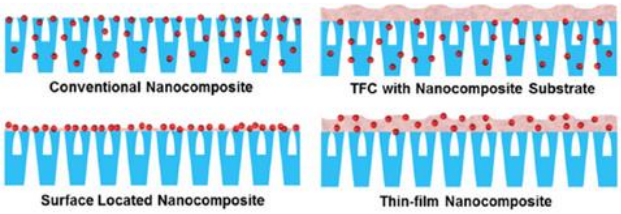

Figure 2.4: Nanocomposite membranes fabricated by different methods [6].

Surface located nanocomposite membranes are studied in order to modify surface properties of the membrane such as hydrophilicity, roughness and charge density. Self-assembly, coating/deposition, chemical grafting, layer-by-layer assembly techniques are commonly used to fabricate surface-located nanocomposite membranes [6]. The fourth category, the "true" thin film nanocomposite membranes are prepared by incorporating nanomaterials into the polyamide layer. This can be achieved by dispersing nanoparticles into the aqueous (MPD) or organic (TMC) phase prior to in-situ interfacial polymerization as shown in Figure 2.5 [6].

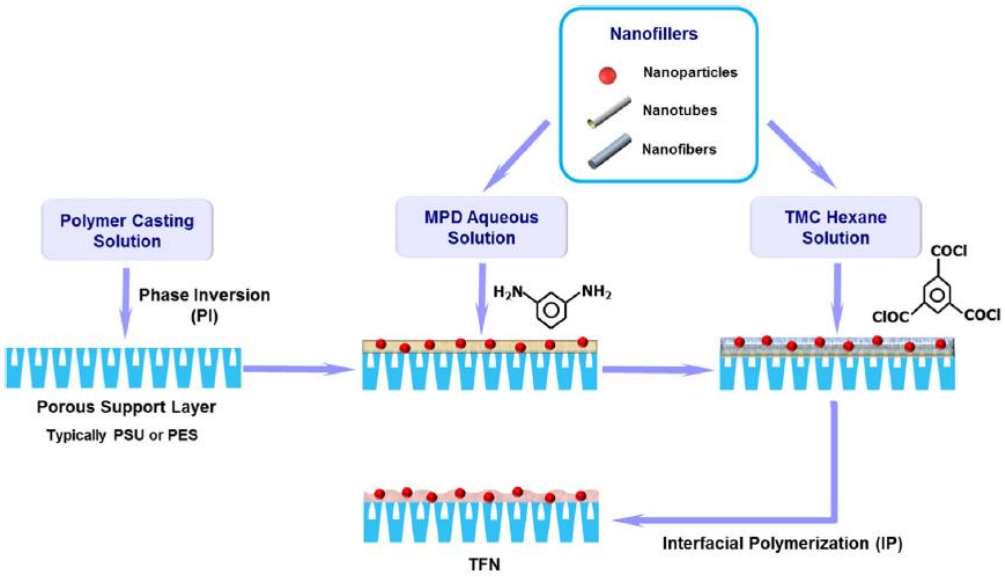

Figure 2. 5: Fabrication of "thin film nanocomposite" membranes [6].

2.3.2 Effect of nanoparticles on membrane structure and performance

In terms of permeability-selectivity trade-off, the most obvious advantage of nanoparticles such as zeolite or aquaporin is that they can provide additional channels which favor the passage of water molecules over solutes. Expression of hydrophilic

nanoparticles on the surface may also increase the hydrophilicity of polyamide [30]. A less obvious but equally important effect is that presence of nanomaterials may alter the chemical structure and morphology of polyamide layer. They may interfere with the reaction between MPD and TMC resulting in reduced degree of crosslinking accompanied by increased water permeability and improved hydrophilicity originating from pendant carboxylic acid groups [6]. Although the incorporated material itself does not have high water permeability, modified polyamide structure is found to have significantly improved water flux in some cases [23]. In order to retain membrane selectivity while increasing permeability, size of the nanoparticles and their interactions with the polyamide are important considerations.

Several studies show that improved surface hydrophilicity originating from hydrophilic nanoparticles such as carbon nanotube, graphene oxide and zeolite can significantly contribute to antifouling properties [31–33]. Furthermore, it is also possible to enable antibacterial properties of composite membranes by incorporating certain biocidal nanomaterials such as silver nanoparticles [34].

Mixed matrix membrane approach may be employed to improve membrane selectivity as well as permeability and antifouling properties. Pores with precise shapes and dimensions can be introduced into nanoparticles or they can be functionalized with certain chemical groups in order to achieve specific molecular separations [35].

2.4 Carbon Nanotubes and Their Desalination Potential

Among nanomaterials used for TFN membrane fabrication, carbon nanotubes (CNTs) stand out due to their unique water permeability properties. They consist of condensed carbon rings forming a graphene layer further rolled up into a perfect cylinder as shown in Figure 2.6. Rolled-up vector (n, m) called chirality is an important characteristic which defines geometric and electronic properties of a CNT. Graphene layers can be arranged in a single-walled (SWNT) or multi-walled (MWNT) structures. There are several CNT fabrication methods such as catalytic chemical vapor deposition (CVD), arc discharge and laser ablation. CVD technique is commonly preferred due to high quality of fabricated CNTs; however, controlling the chirality and producing CNTs with a narrow size distribution is still challenging [8, 35].

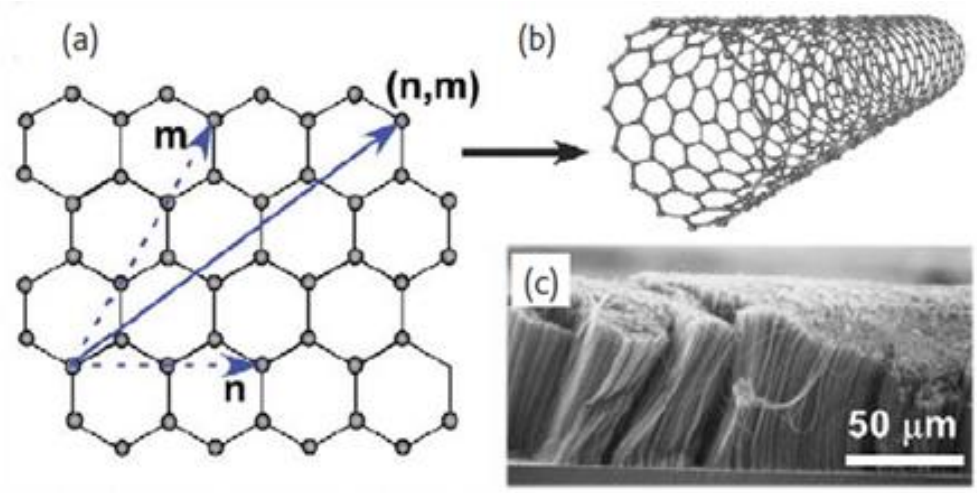

Figure 2.6: Structure and morphology of CNTs. (a) Schematic of a graphene sheet and chirality. (b) Three-dimensional model of a SWNT. (c) A scanning electron microscope (SEM) image of a vertically aligned array of MWNTs [8].

2.4.1 Water and ion transport through CNTs

Water transport in CNTs has attracted great deal of attention due to their highly smooth and hydrophobic walls which greatly reduce the friction. Noy et al. measured water transport rates at least 2-3 orders of magnitude faster than those calculated by Hagen-Poiseuille equation used for no-slip hydrodynamic flow [8]. This surprisingly fast water transport can be attributed to unique re-orientation of water molecules in nanoscale confinements as well as near-frictionless surface of CNTs.

Hummer et al. investigated filling of a (6,6) SWNT with water via molecular dynamics simulation. Water molecules were found to fill nanotube having diameter of 0.81 nm in tens of picoseconds and re-orient in a single-file configuration as shown in Figure 2.7. In order to form this single-file chain and enter into CNT, water molecules have to lose some of their hydrogen bonds formed in bulk water. Loose of hydrogen bonds may be considered thermodynamically unfavorable at first; however, it was found that confinement of water lowers its excess chemical potential, in other words free energy, by narrowing interaction (binding) energy distribution as seen in Figure 2.7. Narrowed interaction energy distribution shows that water molecules populate their energetic ground state with fewer in number but more stable hydrogen bonds [9, 36].

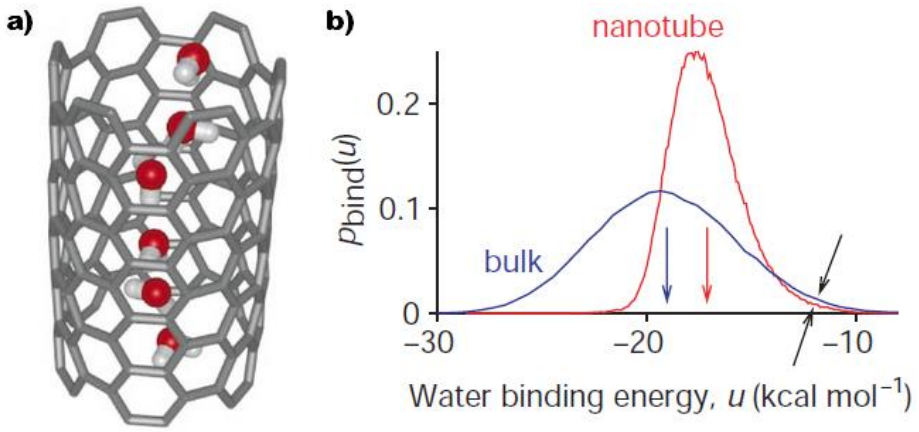

Figure 2.7: Water transport through CNTs. **(a)** Hydrogen-bonded water chain inside the CNT **(b)** Probability distribution of water binding energies for bulk water and water inside the CNT [33].

Simulation studies which investigate water and ion transport through CNTs with different chirality reveal the importance of CNT diameter in terms of permeability and ion exclusion. Since CNT carbons are usually treated as uncharged particles, ion rejection relies essentially on size exclusion. Park pointed out that complete rejection of ions such as K^+, Na^+ and Cl^- requires a diameter of approximately 0.4 nm which corresponds to hydrated ion size. When CNT diameter is small enough to force ions to strip off their first hydration shell, they encounter a high energy barrier [37].

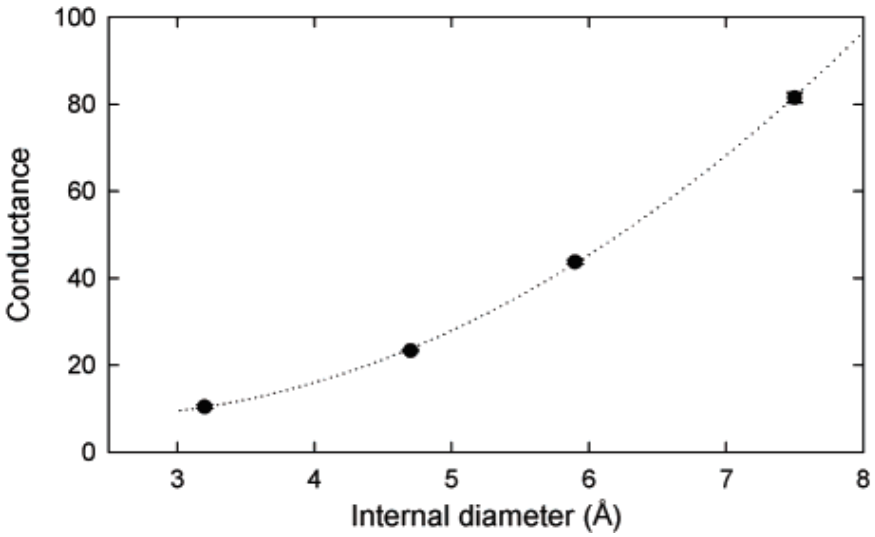

Figure 2.8: Water conductance through SWNTs in water per tube per ns [38].

In line with Park'a argument, Corry found that free energy of ions entering (5,5) and (6,6) SWNTs are high enough to obtain 100% salt rejection whereas energy barrier drastically reduces for (8,8) SWNT which is resulted in 58% salt rejection. Water

permeation is also significantly affected by CNT diameter and conductance is found to increase exponentially as SWNTs diameter increases as shown in Figure 2.8 [38].

2.4.2 Functionalization of CNTs

Since simulation studies show that CNT diameter required for complete ion exclusion is very small for practical applications, functionalization of CNT tips is worthy of attention. Corry studied (8,8) SWNTs functionalized with different groups, namely carboxylate anion (COO^-), amine cation (NH_3^+), hydroxyl (OH) and amide ($CONH_2$). Negative groups improved the rejection of Cl^- ion which has a greater dehydration energy; however, improved rejection of Na^+ requires multiple charged groups (at least four NH_3^+ or eight COO^-) in exchange for water flux reduction. It was also concluded that using a mixture of anionic and cationic groups for CNT functionalization can improve removal of both Na^+ and Cl^- ions with a reasonable water flux decline compared to existing RO membranes [39, 40]. Chan et al. employed zwitterionic groups to improve ion rejection and their simulation studies show that binding two bulk zwitterionic groups having the structure ($-COO-(CH_2)_3-N^+(CH_3)_2-(CH_2)_2COO^-$) to the (20,0) SWNT with diameter of 15.6 Å can result in 100% salt rejection with a significant decrease in water conductance [22].

Experimental studies point out remarkable molecular separation potential of functionalized CNTs as well. Hinds et. al grew vertically aligned MWNT array via Fe-catalyzed chemical vapor deposition process on a quartz substrate and further obtained a freestanding composite CNT-polystyrene thin film. Reactive carboxylic acid groups were introduced selectively from the tips of CNTs via plasma treatment. Untreated and carboxylic acid functionalized CNTs did not show any significant $Ru(NH_3)_6^{3+}$ ion rejection. When biotin molecules were reacted with carboxylate groups with a carbodiimide-mediated reaction, biotin functionalized CNTs decreased $Ru(NH_3)_6^{3+}$ flux by a factor of 5.5 indicating a gate-keeper controlled chemical separation mechanism [41]. Later on, they investigated the effect of different functional groups on the ion rejection of CNT membranes fabricated by the same method. They used a straight chain alkene, anionically charged dye molecule, and an aliphatic amine elongated by polypeptide spacers. Relative selectivity of [MV^{2+}] and [$Ru\text{-}(bipy)_3^{2+}$] ions was found to vary between 1.7 to 3.6 as a function of end groups [42]. Fornasiero et. al used a sub-2-nm CNT membranes to examine the effect of negatively charged

functional groups on the ion selectivity. They vertically aligned DWNTs and deposited silicon nitride followed by uncapping and selective functionalization of CNT tips with hydroxyl (OH), carbonyl (C=O), and carboxylic (COOH) groups via etching process. Nanofiltration experiments carried out under 0.69 bar with 1.0 mM KCl feed solution showed that CNT membranes attained a flux that is an order of magnitude higher than the commercial NF membranes with a corresponding ion rejection. Their results also implied that Donnan-type exclusion mechanism governed by electrostatic interactions was the dominating mechanism in terms of ion rejection [43].

2.5 CNT/Polyamide Thin Film Nanocomposite Membranes

Unique water permeability properties of CNTs made them an excellent nanofiller to study desalination potential of thin film nanocomposite membranes. As discussed for the pure CNT membranes, tip functionalization is an important advantage in terms of selectivity. Another reason why experimental studies widely employ CNT functionalization is that CNTs are treated with carboxylic acid in order to remove fullerene caps and residual catalysts during fabrication steps. In other words, most of the carbon nanotubes used in TFN membrane fabrication are purchased as already-functionalized with carboxylic groups which can serve as target sites for chemical modification. Besides, functionalization with polar groups enable dispersion of CNTs in water or polymer.

The first CNT/polyamide TFN membrane fabrication method was patented by Ratto et. al in 2011. They dispersed SWNTs with diameter of 1.2-1.4 nm in either two phases of interfacial polymerization reaction. As a result, polyamide layer was grown surrounding the randomly oriented CNTs acting as channels for selective passage of water [44]. Method can be considered more scalable compared to other methods in which CNTs are in-situ grown during membrane fabrication. Until date, various studies investigated the desalination performance of CNT/polyamide TFN membranes employing SWNTs or MWNTs functionalized with different molecules and incorporated into polyamide matrix via different methods. Some of these studies are summarized in Table 2.2.

Table 2.2: Studies investigating the desalination performance of interfacially polymerized CNT/polyamide TFN membranes.

Ref. and year	Type of CNT	Loading amount and method	Application	Testing conditions	Water permeance ($L/(m^2\,h)/bar$)	Salt rejection, %
[45] 2011	COOH and OH func. MWNTs	0.1% (w/v) dispersed in aqueous MPD	Reverse osmosis	16 bar 2000 ppm NaCl	1.63 (TFC) 4.44 (TFN)	95.0 (TFC) 82.0 (TFN)
[22] 2013	Zwitterion func. SWNTs OD: 1.5 nm, L: 1 μm	20 wt% in PA filtration through support pores	Reverse osmosis	36.5 bar 2500 ppm NaCl	0.32 (TFC) 1.34 (TFN)	97.6 (TFC) 98.6 (TFN)
[46] 2013	Amine func. MWNTs OD: 2 nm, L: 50 μm	0.05 wt% dispersed in aqueous MPD	Forward osmosis	2.4 bar 20 mM NaCl	3.10 (TFC) 3.60 (TFN)	70.0 (TFC) 89.3 (TFN)
[47] 2014	COOH func. MWNTs ID: 5 nm, L: 1-5 μm	0.1% (w/v) dispersed in aqueous MPD	Reverse osmosis	16 bar 2000 ppm NaCl	0.93 (TFC) 1.75 (TFN)	92.0 (TFC) 90.0 (TFN)
[48] 2014	Thermally oxidized (cap-opened) MWNTs OD: 6-9 nm	0.25 wt% dispersed in aqueous MPD	Reverse osmosis	15.5 bar 2000 ppm NaCl	2.50 (TFC) 2.74 (TFN)	98.7 (TFC) 98.2 (TFN)
[23] 2015	Pristine MWNTs	0.4 wt% dispersed in aqueous MPD	Reverse osmosis	50 bar 35000 ppm NaCl	0.54 (TFC) 1.29 (TFN)	97.0 (TFC) 90.0 (TFN)
[49] 2016	COOH, OH or NH func. MWNTs OD: 10-20 nm	0.1% (w/v) dispersed in aqueous PIP	NF	6 bar 2000 ppm Na_2SO_4	3.33 (TFC) 6.17-8.33 (TFN)	97.0 (TFC) 92.0-95.0 (TFN)

Table 2.2 (continued): Studies investigating the desalination performance of interfacially polymerized CNT/polyamide TFN membranes.

Ref. and year	Type of CNT	Loading amount and method	Application	Testing conditions	Water permeance ($L/(m^2\,h)/bar$)	Salt rejection, %
[50] 2017	COOH func. MWNTs D: 15 nm, L: 15 μm	0.001 wt% dispersed in aqueous MPD	Reverse osmosis	15.5 bar 2000 ppm NaCl	2.39 (TFC) 2.90 (TFN)	98.0 (TFC) 97.0 (TFN)
[51] 2017	Pristine and COOH func. MWNTs D: 3-10 nm, L:20 μm	0.001–0.009 wt% in MPD or 0.001–0.009 wt% in TMC	Reverse osmosis	15.5 bar 2000 ppm NaCl	1.32 (TFC) 2.45-2.77 (TFN)	98.0 (TFC) 94.0-99.0 (TFN)
[52] 2017	Amine func. MWNTs D: 5-20 nm, L: 5μm	0.001-0.05 wt% dispersed in aqueous MPD	Reverse osmosis	15 bar 2000 ppm NaCl	2.80 (TFC) 2.33-3.87 (TFN)	95.0 (TFC) 95.0-97.5 (TFN)
[53] 2017	Pristine, COOH or NH_2 func. SWNTs D: 3.5 nm L: 5-30 μm	0.05 wt% dispersed in aqueous MPD	Reverse osmosis	20 bar 2000 ppm NaCl	1.10 (TFC) 1.50-1.75 (TFN)	98.0 (TFC) 97.5-99.0 (TFN)
[54] 2017	Zwitterion func. MWNTs D: 8-15 nm, L: 2 μm	0.005-0.05 wt% dispersed in aqueous PIP	NF	6 bar 1000 ppm NaCl	11.67 (TFC) 12.0-15.0 (TFN)	50.0 (TFC) 20.0-30.0 (TFN)

2.6 Asparagine and ACA Amino Acids

2.6.1 Aquaporin channels and asparagine

Biomimetic desalination membranes often employ remarkable water permeability and ion rejection properties of biological aquaporin channels by directly incorporating them into the membrane structure [5]. Unique structure of aquaporin proteins also inspired design of artificial water channels consisting of self-assembled dendritic dipeptides or unimolecular pillar[5]arene derivatives [11].

In 2003, Peter Agre was awarded with Nobel Prize in chemistry for his discovery of aquaporin water channels. When the lipid bilayer structure of biological cell membranes was discovered in 1920s, the main mechanism of water transport was presumed to be simple diffusion through the cell membrane. After a while, it was accepted that water transport in certain tissues such as renal tubule, secretory glands or red blood cells was very high and could not be explained by simple diffusion. Scientists predicted the existence of special water-selective channels in these membranes but neither the constituents of the channels could be identified nor the transport mechanism was understood until the work of Agre. He successfully isolated the channel protein "aquaporin" and proved its function. Then three dimensional structure of the tetrameric channel was resolved with the help of X-ray and molecular dynamic simulation studies [10].

Ability of channel to effectively exclude ions while allowing passage of water relies on two so-called selectivity filters as depicted in Figure 2.9. Water is present in the form of bulk solution in extracellular and intracellular sides of the hourglass channel. The narrowest pore having diameter of 2.8 Å is located at the center where positively charged arginine (R_{195}) side chain repels protons and water molecules are re-oriented in a single-file configuration losing their hydrogen bonds to fit this space. The second barrier includes two highly conserved asparagine residues (N_{192} and N_{76}) which transiently form hydrogen bonds with water molecules and allow water to move without resistance [10, 55].

It was suggested that asparagine residues also play an important role in ion exclusion in addition to favoring passage of water molecules. Wree et al. mutated the asparagine to serine residue in order to investigate requirement of asparagine in NPA sequence

for cation exclusion. It was found that mammalian AQP1 N76S mutants leaked sodium ions [56]. A similar sodium leak was observed in AQP1-N192D mutants where asparagine residue was converted to aspartate [57].

Similarities between CNTs and aquaporin channels are well worth the attention: inner cavity of aquaporin is lined with hydrophobic residues which can be related with hydrophobic interior surface of CNTs. Re-orientation of water molecules confined into aquaporin and CNT is also similar. In order to take this similarity a step further, asparagine residue is used to functionalize CNTs in this study. Effect of high hydrogen bonding capacity and ion exclusion ability of asparagine on the water permeability and salt rejection is investigated.

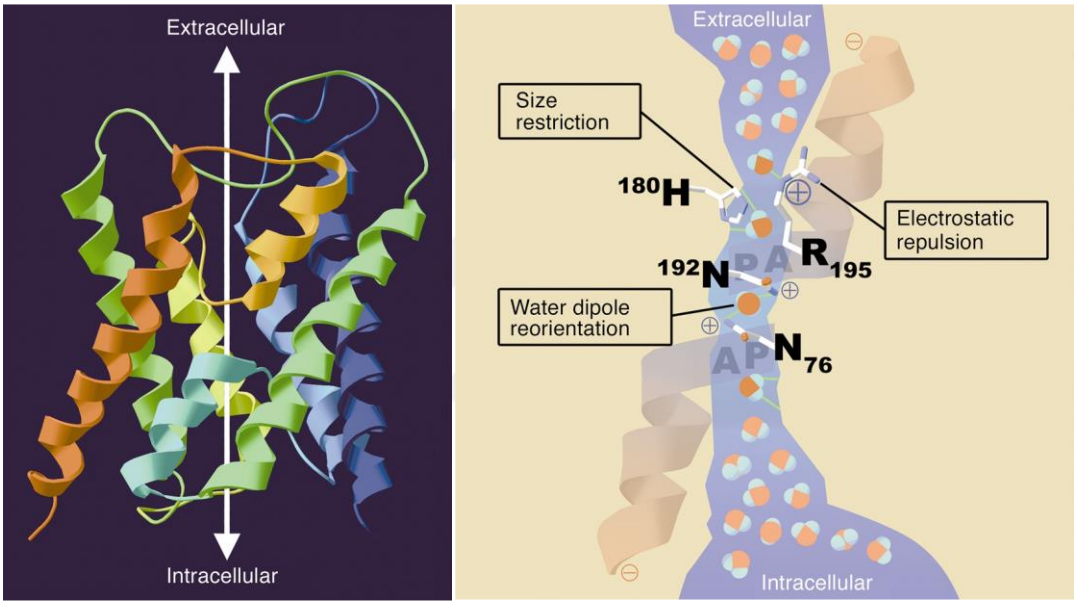

Figure 2.9: Tetrameric structure and selectivity filter of aquaporin [55].

2.6.2 8-amino caprylic acid (ACA)

8-amino caprylic acid (ACA) was used by Majumder et al. to functionalize CNTs in order to investigate the effect of tip functionalization on the ion rejection. It was preferred due to relatively large molecular size in order to examine effect of steric hindrance on water permeability and salt rejection.

3. EXPERIMENTAL STUDY

As-received (COOH functionalized) SWNTs were further functionalized with asparagine (Asn) and 8-amino caprylic (ACA) amino acids through carbodiimide mediated reaction between carboxylic groups on CNTs and primary amines in amino acids. Functional CNTs were characterized with TGA, XPS and Raman spectroscopy. For the fabrication of TFN membranes, CNTs were dispersed in water and vacuum-filtered through the pores of support membrane. Interfacial polymerization of MPD and TMC were carried out in the absence or presence of CNTs. Structure and morphology of resulting membranes were characterized by FTIR, XPS, FESEM, AFM and contact angle measurements. Polarized Raman spectroscopy was used to investigate CNT aligment inside the polymeric matrix. Separation performance was examined using cross-flow filtration system.

3.1 Functionalization and Characterization of CNTs

3.1.1 Functionalization of CNTs

SWNTs purchased from Nanografi Co. Ltd. were fabricated by CVD and already functionalized with carboxylic acid (COOH). Technical specifications reported by the manufacturer was presented in Table 3.1. SEM and TEM images shown in Figure 3.1 was also provided by the manufacturer.

Table 3.1 Technical specifications of SWNTs reported by the manufacturer.

Purity	> 92 wt%
Average diameter	1 nm
Internal diameter	0.8 - 1.6 nm
Outer diameter	1 - 2 nm
Length	1 - 3 μm
Density	2.2 g/cm^3
G/D ratio	8
Ash content	1.5 wt%

The following chemicals were used for the functionalization of CNTs with Asn and ACA without further purification: MES monohydrate (2-(N-morpholino)-ethanesulfonic acid, Sigma Aldrich, ≥99.5%), EDC (1-ethyl-3-(3-dimethylaminopropyl) carbodiimide hydrochloride, Thermo Fisher), ACA (8-amino octanoic acid, Sigma Aldrich, 99%), L-Asparagine (Sigma Aldrich, ≥98%). In addition, Millipore 47 mm stainless steel filtration system and Millipore-Durapore PVDF membrane filter having pore size of 0.1 μm were used for washing and filtering CNTs.

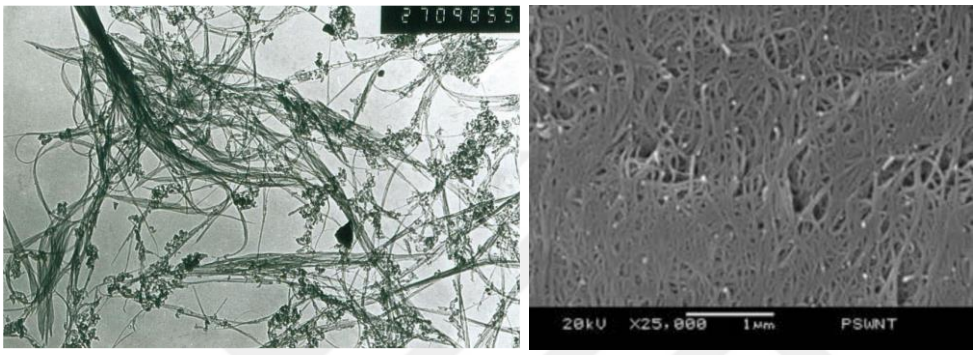

Figure 3.1: TEM (left) and SEM (right) images of SWNTs provided by manufacturer.

Structure of amino acids used for functionalization is shown in Figure 3.2. EDC was used as cross-linker in order to activate carboxyl groups on the CNTs and reacted with primary amines of amino acids. Reaction was schematically shown in Figure 3.3 and details of the experimental procedure is given below. The same procedure was used for functionalization of CNTs with biotin and ACA molecules in the literature and it was adapted for Asn functionalization in this study [41, 42, 58].

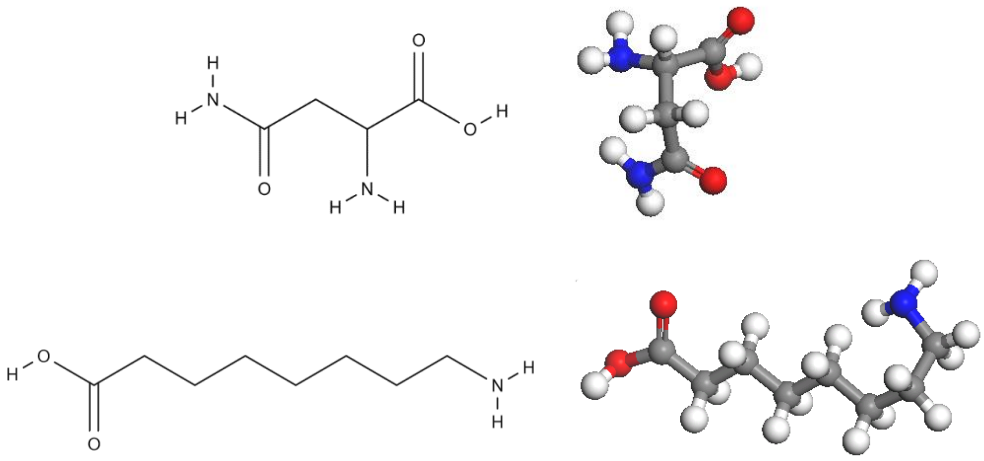

Figure 3.2: Structure of Asparagine (top) and ACA molecules (bottom).

Functionalization with Asn:

- 6 grams of MES monohydrate was dissolved in 280 ml of water to prepare 0.1 M MES buffer solution.
- 50 mg of COOH-CNT was added to 250 ml of MES buffer and probe-sonicated in ice-water bath for 10 minutes.
- 0.13 mg asparagine was dissolved in 1 ml MES buffer to prepare 1 mM Asn solution.
- 239.25 mg EDC was dissolved in 25 ml MES buffer to prepare 50 mM EDC solution.
- 25 ml of EDC solution is added to CNTs and sonicated in ultrasonic bath for 2 hours in room temperature.
- 625 μL of Asn solution is added to reaction mixture and sonicated for 2 hours.
- Mixture is filtered through membrane filter and washed with DI water. Resulting black residue is dried in vacuum oven in room temperature.

Functionalization with ACA:

- 6 grams of MES monohydrate was dissolved in 280 ml of water to prepare 0.1 M MES buffer solution.
- 50 mg of COOH-CNT was added to 250 ml of MES buffer and probe-sonicated in ice-water bath for 10 minutes.
- 0.16 mg ACA was dissolved in 1 ml MES buffer to prepare 1 mM ACA solution.
- 239.25 mg EDC was dissolved in 25 ml MES buffer to prepare 50 mM EDC solution.
- 25 ml of EDC solution is added to CNTs and sonicated in ultrasonic bath for 2 hours in room temperature.
- 625 μL of ACA solution is added to reaction mixture and sonicated for 2 hours.
- Mixture is filtered through membrane filter and washed with DI water. Resulting black residue is dried in vacuum oven in room temperature.

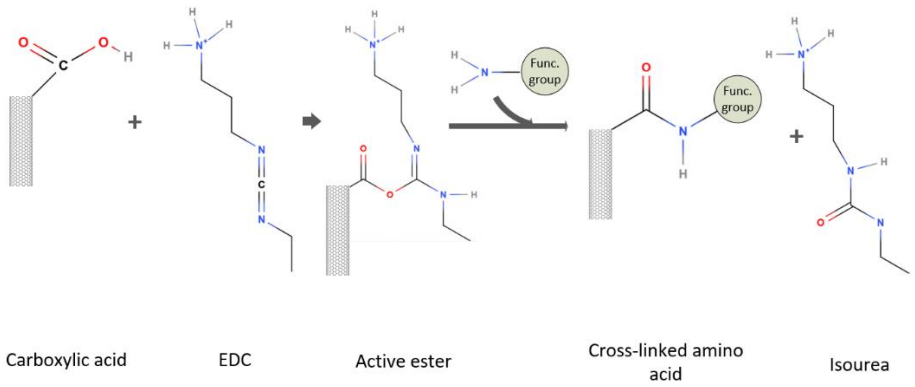

Figure 3.3: Schematic representation of Asn and ACA functionalization.

3.1.2 Characterization of functionalized CNTs

In order to characterize as-received COOH functionalized CNTs and to monitor effects of amino acid functionalization, TGA, XPS and Raman analysis were carried out.

Thermal gravimetric analysis (TGA) measures the weight loss of a sample as a function of temperature and time under controlled atmosphere. TGA analysis provides information about decomposition or oxidation of a material as well as its volatile constituents. In this study, TGA measurements were used to show conversion of COOH groups to Asn and ACA groups. Temperature of CNT sample (2-10 mg) was increased to 800ºC with oxygen feed rate of 100 cm^3/min and heating rate of 5ºC/min. Weight loss was recorded.

In X-ray photoelectron spectroscopy (XPS) which is a quantitative spectroscopic technique, core level electrons of atoms present at the surface of the material are excited and their binding energy is determined. Type of atoms and bonds constituting the material can be detected from XPS spectrum. Besides, it is possible to calculate fractions of these atoms by measuring the areas under intensity peaks. In this study, as-received CNTs were analyzed first in order to determine concentration of COOH groups. Then, functionalized CNTs were analyzed and fraction of nitrogen atoms, which must come from amino acids, was determined to calculate fractional conversion.

Finally, Raman spectroscopy was used for the characterization of as-received and amino acid functionalized CNTs. It is possible to measure intensity of G band and D band for quantitative analysis of deformations. All carbon atoms in SWNTs vibrate between wavelengths of 150-350 cm^{-1} depending on the tube diameter. These low energy vibrations are called radial breathing mode. Tangential modes with high energy occur at 1600 cm^{-1} and peak observed at this characteristic wavelength is called G

band. The second peak observed just below G band around 1300 cm^{-1} is referred to as D band in the literature and known to originate from deformations in CNTs. Higher G/D ratio indicates low concentration of defects. [59, 60]. Raman spectroscopy was used to evaluate effect of amino acid functionalization on CNT stability in this study.

3.2 Synthesis of Thin Film Composite (TFC) Membranes

3.2.1 Preparation of support layer

A commercial polysulfone UF membrane (Alfa Laval GR40PP) having 100 kDa molecular weight cut off was used as support layer. Since commercial membranes are coated with a protective glycerol layer, support layer was subjected to a cleaning process prior to use for removal of glycerol layer and opening of pores. Sodium dodecyl benzene sulfonate (SDBS) treatment was also carried out to swell the polymer and increase hydrophilicity as recommended in the literature [22]. The cleaning procedure was as follows:

- Soaking in DI water overnight
- Soaking in 0.25% (v/v) sodium bisulfite solution for 2 days and washing with DI water
- Soaking in dilute acidic HNO_3 solution (pH=2.5-3) for 2 hours and washing with DI water
- Soaking in dilute basic NaOH solution (pH=9-10) for 2 hours and washing with DI water
- Soaking in 0.5% (w/v) SDBS solution for 2 days
- Washing with DI water and soaking in DI water overnight to remove residual SDBS.
- Keeping in DI water in refrigerator.

3.2.2 Formation of polyamide layer

Formation of polyamide layer on top of the support was carried out via interfacial polymerization using following materials without further purification: MPD (m-phenylenediamine, Sigma Aldrich, ≥%99), TMC (1,3,5-Benzenetricarbonyl trichloride, Sigma Aldrich, %98), SDBS (sodium dodecyl benzenesulfonate, Sigma Aldrich), triethylamine (TEA, ≥%99.5), n-hexane (Merck, >%95%).

Since the MPD and TMC monomers were highly sensitive to moisture and light, solutions were prepared in glove-box under conditioned Argon atmosphere. While aqueous phase contained 2% (w/v) MPD, 2% (w/v) TEA and 0.04% (w/v) SDBS, organic phase contained 0.5% (w/v) TMC and hexane. Solutions were stirred via magnetic stirrer for at least 30 minutes. A circle having diameter of 90 mm was cut from the support membrane, washed with DI water and placed in Millipore 90 mm glass filtration system shown in Figure 3.4. MPD solution is introduced from the top and support layer is soaked for 20 minutes. Then support was taken out and excess MPD solution was removed by means of a glass roller until no visible droplets stayed on the surface. Filtration system was reassembled, MPD-soaked surface of the support layer was brought into contact with TMC solution for 90 seconds for polymerization reaction to occur. Lastly, resulting TFC membrane was dried in oven at 68°C to remove residual hexane.

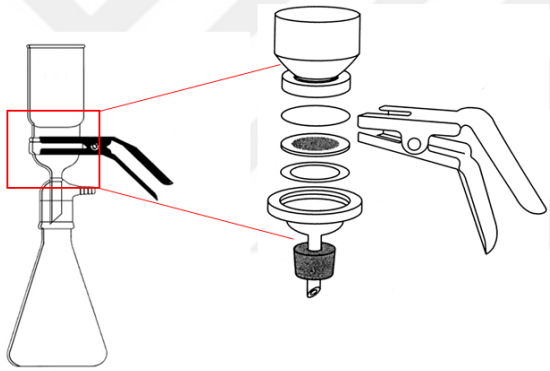

Figure 3.4: Millipore 90 mm glass filtration system.

3.3 Synthesis of Thin Film Nanocomposite (TFN) Membranes

Synthesis of CNT incorporated TFN membranes consists of two steps. First, CNTs were dispersed in water and cleared of from impurities and large bundles. Then they were vacuum-filtrated through the pores of support layer in order to enable partial alignment of CNTs. Second, selective polyamide layer is synthesized on top support in the presence of CNTs via interfacial polymerization.

3.3.1 Preparation and vacuum filtration of CNTs

It is important that CNTs are well dispersed in water and homogeneously embedded in support layer in synthesis of TFN membranes. Precise control of CNT chirality and diameter during the fabrication is difficult and manufacturer reported properties of

CNTs are usually average values. As-received CNT batches may contain CNTs having diameter greater than 1 nm, CNTs that grown together and forming bundles during CVD fabrication and carbonaceous impurities. Presence of large bundles may disrupt the integrity of the polyamide layer and cause serious defects. The following method was employed in order to remove undesired bundles and impurities and homogenously disperse CNTs:

- A previously determined amount of CNT and 10 mg SDBS surfactant were dispersed in 40 ml DI water in ultrasonic bath for 30 minutes and waited overnight for SDBS molecules to surround and swell CNTs.
- Mixture was dispersed via probe-sonication for 30 minutes in ice-water bath as shown Figure 3.5. A sample of 1 ml was spared and its absorbance was measured at wavelength of 500 nm via UV-VIS spectrophotometer. A calibration curve was obtained by serial dilution.
- Sonicated CNT-water mixture was centrifuged at 14,000 rpm for 30 minutes and supernatant was recovered. Before-and-after centrifugation photos were shown in Figure 3.6. Absorbance of supernatant was measured and its CNT concentration was determined via calibration curve. Mixture was diluted if necessary in order to reach desired concentration.
- CNT-water mixture was filtrated through support layer using Millipore 90 mm glass filtration system by applying approximately 50 kPa vacuum as shown in Figure 3.7.

Figure 3.5: Sonication of CNT-SDBS-water mixture on ice-water bath.

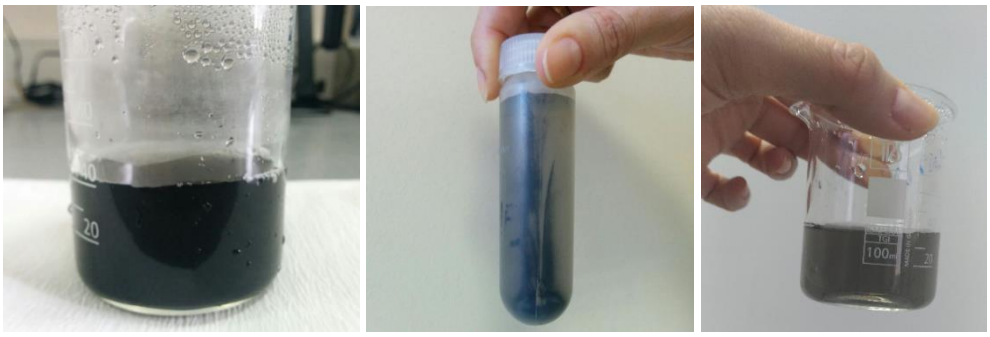

Figure 3.6: Probe sonicated CNT mixture, CNT precipitation formed after centrifugation and recovered supernatant.

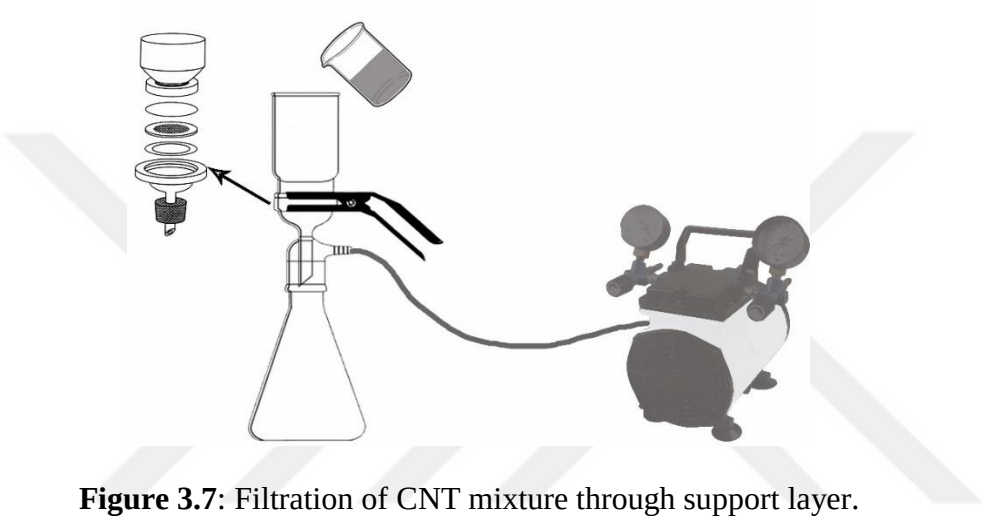

Figure 3.7: Filtration of CNT mixture through support layer.

The CNT amount incorporated into TFN membrane was examined as a parameter in the experimental study. Even though the CNT amount which was dispersed in water at the beginning was known, it was not possible to estimate ratio of precipitated CNT bundles and concentration of supernatant phase recovered from centrifugation. Besides, functional groups might affect dispersion dynamics. Therefore, CNT-water mixture with known concentration was used to obtain a calibration curve. Absorbance of the sample was measured at the wavelength of 500 nm where the characteristic peak of SWNTs was observed in the literature [61]. Then serial dilution was carried out and linearity of calibration curve was monitored. Figure 3.8 represents an example calibration curve.

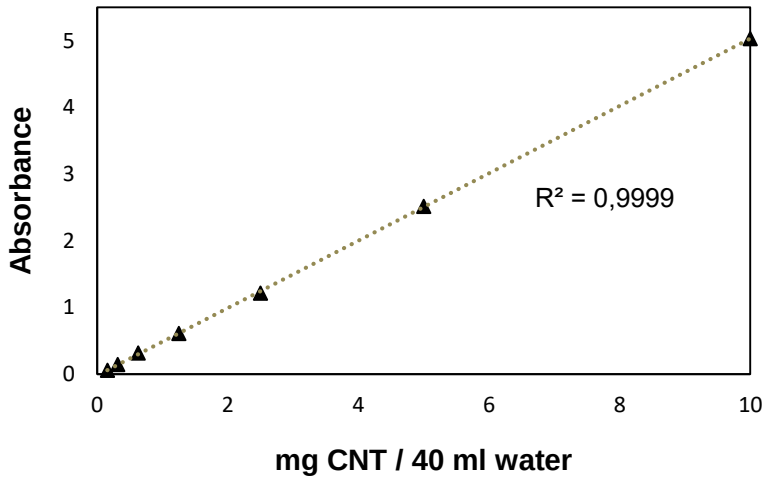

Figure 3.8: A calibration curve to determine CNT concentration of supernatant.

CNT concentration in synthesized TFN membranes was given in number of CNTs per unit membrane area for convenience. An ideal CNT with a chiral vector of (8,8), diameter of 1.085 and length of 2000 nm contains 2.6×10^5 carbon atoms and mass of this CNT can be calculated as 5.18×10^{-15} mg. Taking active area of synthesized membranes is 40 cm^2, CNT amounts used in experiments and corresponding number of CNTs per unit area values are shown in Table 3.2.

Table 3.2: CNT amounts used in experimental study.

CNT concentration (mg/40 ml)	5.00	2.50	1.25	0.62
Number of CNTs ($x10^{-13}$/cm^2 membrane)	2.4	1.2	0.6	0.3

3.3.2 Formation of polyamide layer

After filtration of CNTs through the pores of support layer, selective polyamide layer was synthesized via interfacial polymerization. Procedure is identical to one described in Section 2.2.2.

3.4 Characterization of TFC and TFN Membranes

Fourier Transform Infrared Spectroscopy (FTIR) examines the vibrational modes of molecules and provides information about the course of a reaction via broken and formed chemical bonds. Surfaces of support layer and TFC membranes were analyzed by FTIR to confirm the formation of polyamide layer.

X-ray photoelectron spectroscopy (XPS) was used for the analysis of chemical bonds and atomic composition of polyamide surface. Cross-linking ratio of TFC and TFN membranes was quantitatively determined using XPS.

Scanning Electron Microscopy (SEM) uses focused electron beams to image surface of solid materials in high magnification rates. Surface and cross sectional morphology of the synthesized TFC and TFN membranes was observed via SEM. Zeiss Ultra Plus Field Emission Scanning Electron Microscope was used for imaging. Membrane samples were coated with carbon in order to decrease charging. For imaging of cross-section, samples were frozen in liquid nitrogen and cut.

Atomic Force Microscopy (AFM) is used to scan the surface of samples via a probe at atomic level to obtain high resolution morphological information. Bruker Dimension Icon Atomic Force Microscope was used for the analysis of TFC and TFN surfaces. Membrane areas of 10 μm^2 were scanned in tapping mode to calculate surface roughness in nanoscale.

Water contact angle measurement is a fast and easy technique to examine surface hydrophilicity. Water contact angle may depend on the interaction between the molecules on the sample surface and water as well as surface morphology and roughness. In case of contact angles smaller than 90°, membrane surface is referred to as hydrophilic. Water contact angle measurements were carried out to evaluate effect of CNTs on the surface hydrophilicity via KSV Attension Theta Optical Tensiometer.

Alignment of CNTs inside the polymeric matrix was examined using Polarized Raman Spectroscopy. Intensity of Raman signal belonging to tangential mode of CNTs observed at wavenumber of 1591 cm^{-1} depends on the polarization of laser. When polarization of laser beam directed to membrane surface is parallel to CNT axis (0° or 180° polarization) intensity of the peak is maximum. Similarly, minimum peak intensity is observed in case of perpendicular polarization (90° polarization) [62], [63]. Renishaw İnvia Raman Microscope was used to examine CNT alignment in a TFN membrane sample at parallel and perpendicular polarizations using 633 nm laser.

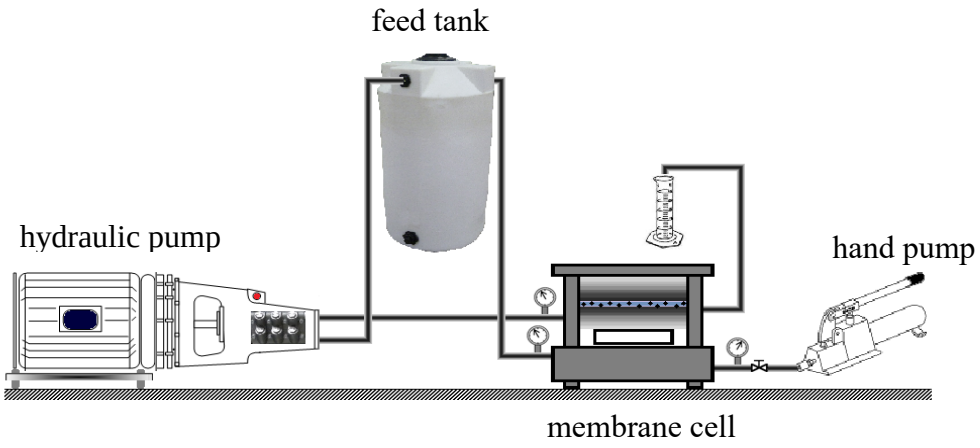

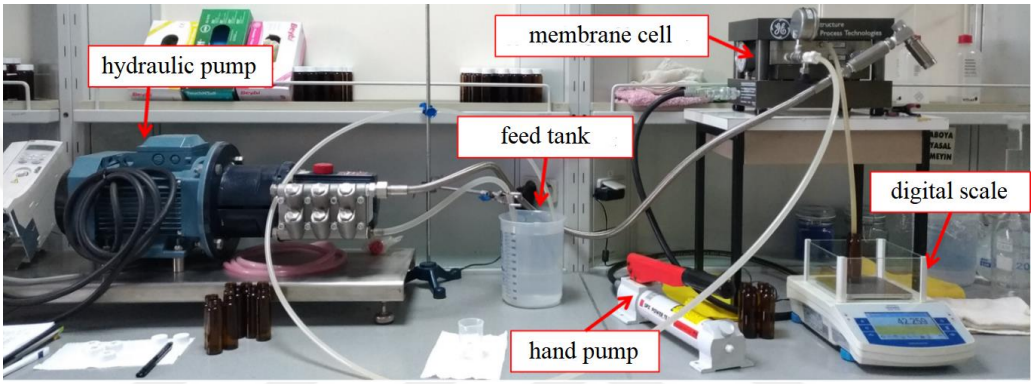

Figure 3.9: Cross flow filtration system used for separation tests.

Finally, the separation performance of TFC and TFN membranes were determined using GE Osmonics Sepa CF cross flow filtration system. System consists of a stainless steel membrane cell, a high pressure hydraulic pump (Hydra-Cell 70 bar), a hand pump used to pressurize membrane cell and feed tank as shown in Figure 3.9. In addition, a digital scale was connected to system to weigh and record mass of permeate as a function of time for calculation of water flux. Membrane cell of the system is designed for a membrane with active area of 140 cm^2; however, active area of membranes synthesized in this study was 40 cm^2. Therefore, membranes were masked with 3M 425 acrylic adhesive aluminum foil prior to performance tests as shown in Figure 3.10.

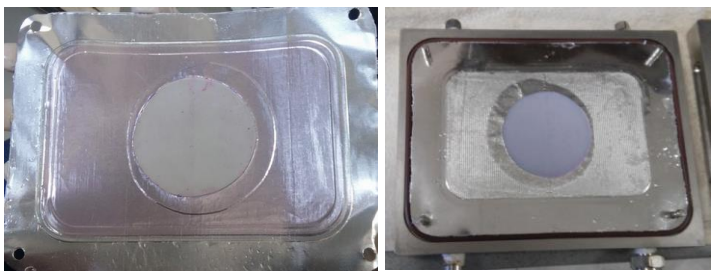

Figure 3.10: Aluminum foil masking of membranes placed in cell.

Membrane was compacted at 16 bar for approximately one hour and it was waited until steady state conditions were achieved before measurements. For the calculation of water flux, pure water was filtrated and following equation, where V_p is the permeate volume (L), A is the active membrane area (m^2), t is time elapsed until permeate sample was collected (h), was used to calculate water flux in LMH:

$$Water\ Flux = \frac{V_p}{A\ x\ t} \tag{3.1}$$

Separation performance of membranes are usually reported at 15.5 bar transmembrane pressure and feed solution containing 2000 ppm NaCl. Therefore, filtration experiments to measure salt rejection were carried out under these conditions. Temperature and pH of the feed solution was 25-27°C and 6-6.5, respectively. Conductivity of the feed and permeate samples was determined using WTW Inolab conductometer and salt rejection, R, was calculated using the following equation where G_p is the conductivity of permeate and G_f is the conductivity of feed sample.

$$R = \left(\frac{G_p}{G_f}\right) x100 \tag{3.2}$$

4. RESULTS AND DISCUSSION

4.1 Characterization of Functionalized CNTs

TGA, XPS and Raman analysis were carried out to examine the effect of functional groups on CNT structure and stability. TGA curves of Asn functionalized CNTs (Asn-CNT) and ACA functionalized CNTs (ACA-CNT) compared to carboxylic acid functionalized CNTs (COOH-CNT) were given in Figure 4.1.

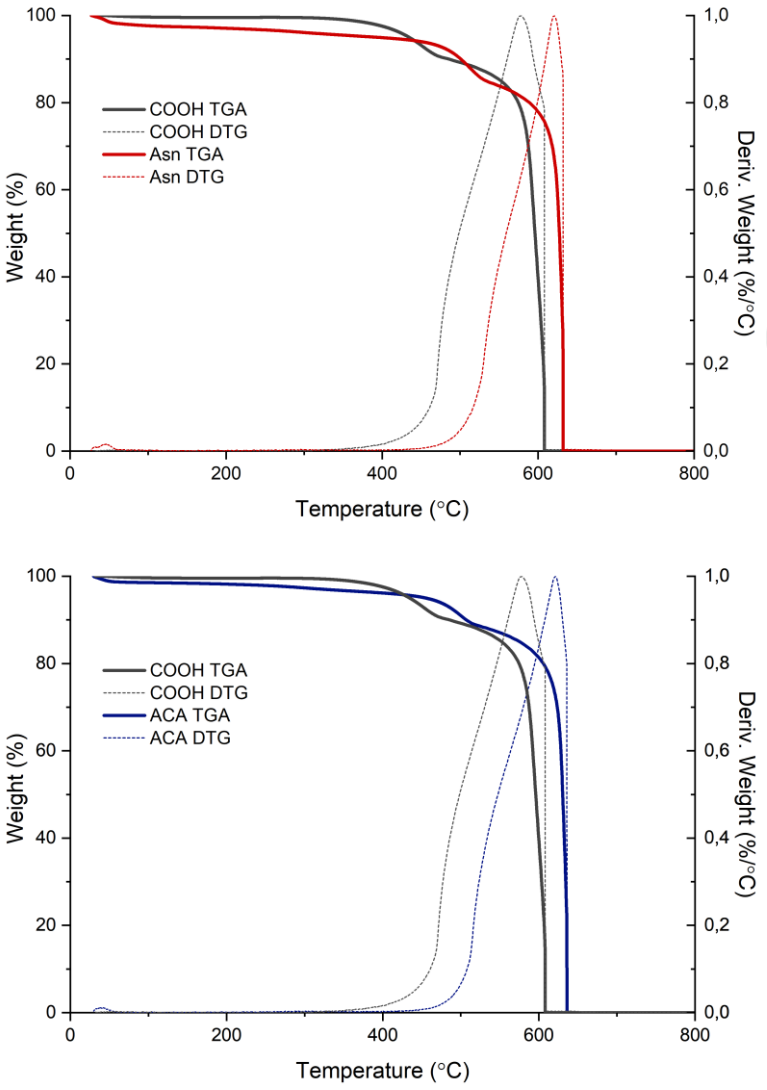

Figure 4.1: TGA analysis of functionalized CNTs.

In TGA analysis of CNTs, weight loss around 100°C is often related to vaporization of solvents while weight loss between 200-400°C is referred to as decomposition of amorphous carbon. Decomposition of sp2 hybridized carbon atoms belonging to SWNT takes place around 600°C [64]. As seen in Figure 3.1, amorphous carbon content of CNTs used in experimental study was low and decomposition temperature is in accordance with the literature. Weight loss observed around 450-490°C was attributed to decomposition of functional groups. Both TGA and DTG curves indicated that functionalization with Asn and ACA affected the thermal stability and resulted in a shift to higher decomposition temperatures.

XPS analysis was used to detect oxygen and nitrogen atoms which was not present in the pristine SWNT structure. It was assumed that these atoms originated from carboxyl and amino acid functional groups. XPS spectra belonging to COOH-CNT, Asn-CNT and ACA-CNT samples were shown in Figure 4.2 and atomic fractions were presented in Table 4.1. Only carbon and oxygen atoms was detected in COOH-CNTs while nitrogen atoms were also observed in addition to carbon and oxygen in amino acid functionalized CNT samples. Atomic composition obtained by XPS analysis were used to calculate conversion ratio of carboxyl groups to amino acids.

Table 4.1: Atomic composition of functionalized CNTs obtained by XPS analysis.

Functional group	C (1s)	N (1s)	O (1s)
COOH	89.10	-	10.90
Asn	86.37	0.79	12.84
ACA	89.60	0.54	9.86

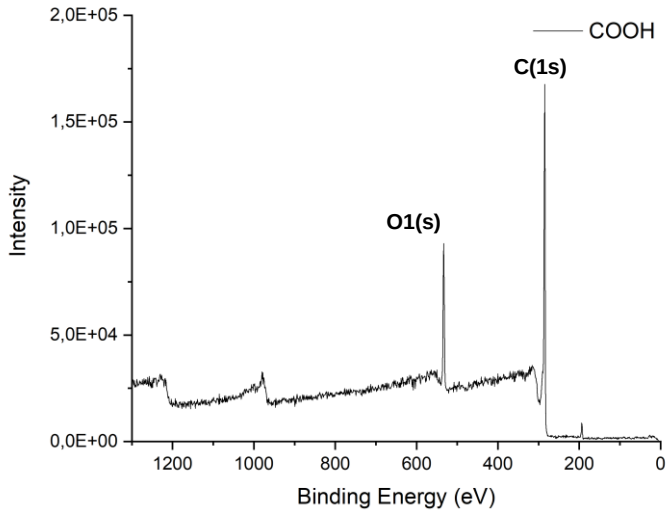

Figure 4.2: XPS spectra belonging to functionalized CNTs.

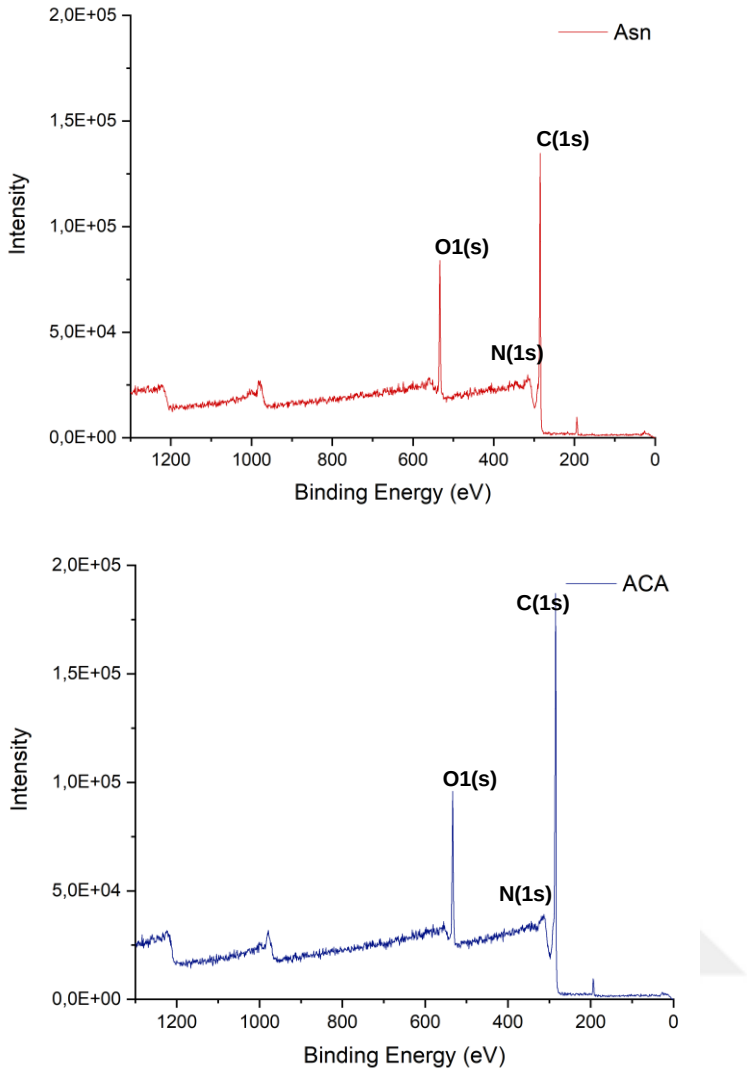

Figure 4.2 (continued): XPS spectra belonging to functionalized CNTs.

SWNTs used in experimental study have an average diameter of 1 nm and length of 2000 nm. Length of the unit cell of an ideal (8,8) CNT with diameter of 1.085 nm is 0.246 nm and number of carbon atoms in this unit cell is equal to 32 as shown in Figure 4.3. Then, a CNT with length of 2000 nm contains $\frac{32}{0.246} x2000 = 2.6x10^5$ carbons.

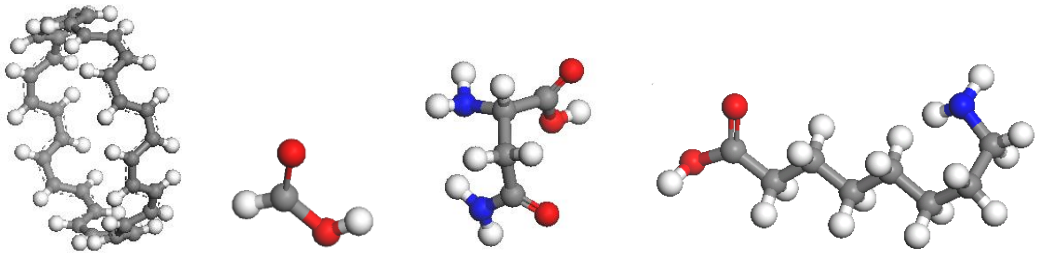

Figure 4.3: Structure of CNT unit cell, COOH, Asn and ACA molecules, respectively.

Calculation of number of COOH groups in CNT:

Since there are 1 carbon and 2 oxygen atoms in a COOH group, 89.1 carbon atoms correspond to 5.45 COOH groups. Number of COOH groups in a single CNT, x, can be calculated from the following equation: $\frac{x}{2.6x10^5+x} = \frac{5.3}{89.1}$ as x=16940.

Calculation of number of Asn groups in CNT:

Similarly, 86.37 carbon atoms correspond to 0.395 Asn groups since there are 4 carbon and 2 nitrogen atoms in an asparagine molecule. From the equation $\frac{x}{2.6x10^5+4x} = \frac{0.395}{86.37}$, number of Asn groups in a single CNT can be calculated as x=1211. In addition, conversion ratio of COOH to Asn can be calculated as 7.15%.

Calculation of number of ACA groups in CNT:

According to Table 3.1, 89.6 carbon atoms correspond to 0.54 ACA groups since there are 8 carbon and 1 nitrogen atoms in an ACA molecule. From the equation $\frac{x}{2.6x10^5+8x} = \frac{0.54}{89.6}$, number of ACA groups in a single CNT can be calculated as x=1646. In addition, conversion ratio of COOH to ACA can be calculated as 9.72%.

Lastly, Raman spectrometry was used to examine effect of functionalization on deformation concentration and stability of CNTs. Raman spectra of COOH and amino acid functionalized CNTs is shown in Figure 4.4. Although G/D ratio slightly decreased with the addition of functional groups, sp2 hybridization and ring structure of CNT carbons were preserved. There are TFN membrane fabrication studies employing CNTs with similar G/D ratios in literature [65].

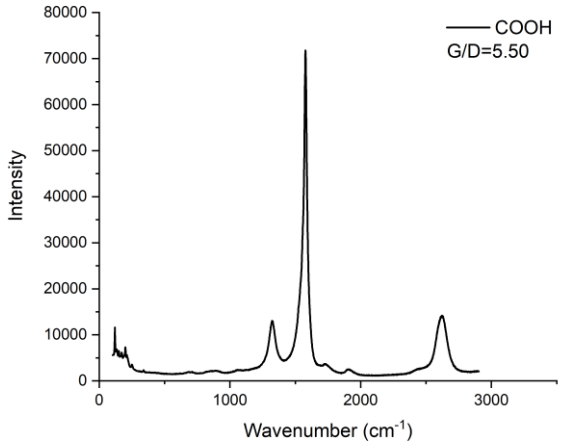

Figure 4.4: Raman spectra and G/D ratios of functionalized CNTs.

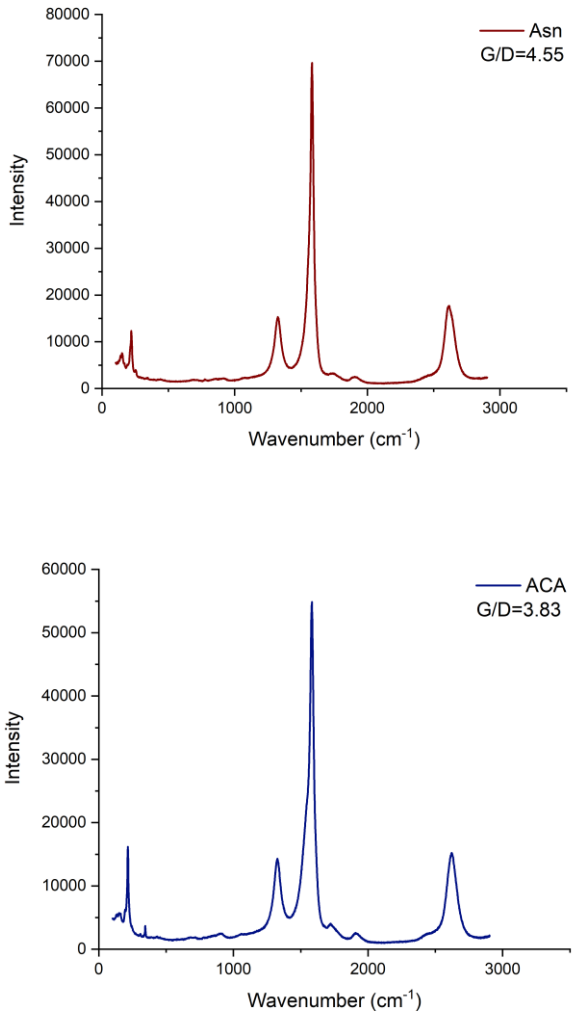

Figure 4.4 (continued): Raman spectra and G/D ratios of functionalized CNTs.

Ideally, functional groups bind to CNT tips only to create the optimum steric hindrance in terms of water flux and salt rejection. However, defects present on CNT sidewalls may allow binding of functional groups to these points as well. In addition to defects formed during the fabrication process, acid treatment applied during cleaning, shortening and functionalizing with COOH also introduce sidewall defects into CNTs. CNTs used in this study was purchased as COOH functionalized, and high oxygen content as well as relatively low G/D ratio indicated high defect concentration. Therefore, it was not possible to control how many amino acid molecules were bonded to CNTs and where they were bonded. Excess amount of amino acids was added to reaction medium and conversion ratio was roughly estimated from XPS analysis. Since Asn and ACA ratio is lower than COOH, it might be assumed that number of amino acids bonded to sidewalls is lower compared to COOH. In addition, all the oxygen

content was assumed to originate from COOH while conversion ratios were calculated. However, lactonic and phenolic groups might be also formed during fabrication of CNTs as shown in Figure 4.5 [66]. These groups do not participate in functionalization reactions but they still contribute to oxygen content of CNT samples.

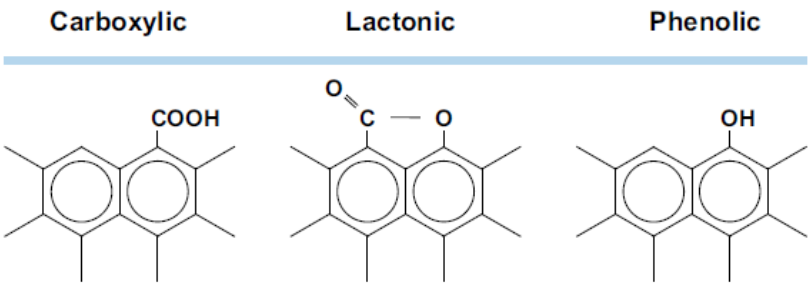

Figure 4.5: Functional groups that may be formed during fabrication and post-treatment of CNTs [66].

4.2 Optimization and Characterization of Polyamide Layer

Properties of the support layer is an important factor affecting the formation of polyamide layer. Optimized interfacial polymerization conditions may vary depending on pore size and distribution of support layer. For instance, a substrate with smaller pores may result in a thicker polyamide layer compared to another substrate with larger pores even though monomer concentrations and reaction time are identical. In this study, support membrane was selected based on the minimum pore size required for embedding of SWNT bundles. Based on filtration experiments and SEM images, a commercial polysulfone UF membrane (Alfa Laval GR40PP) having MWCO of 100 kDa and average pore diameter of 60 nm was selected. SEM images of support membrane surface and cross section are shown in Figure 4.6.

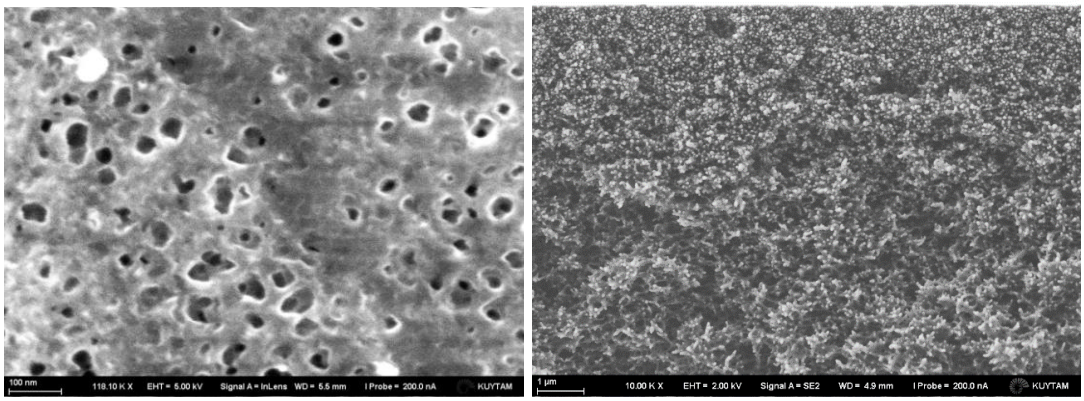

Figure 4.6: Surface and cross section SEM images of support layer.

After selection of support layer, conditions of interfacial polymerization reaction was optimized accordingly. In literature, monomer concentrations of 2 wt% MPD and 0.1-0.15 wt% TMC were recommended for a highly crosslinked polyamide layer [18]. However, these TMC concentrations resulted in a very thin polyamide layer with defects and salt rejection decreased to below 90%. Large pore size of the support layer used in this study required a higher concentration of TMC (0.5 wt%) in order to form a defect free polyamide layer which was thick enough to host CNTs. Addition of TEA as acid acceptor to aqueous phase is recommended to neutralize reaction medium [17]. Addition of SDBS surfactant to aqueous solution did not have a significant effect on TFC membrane structure and performance; however, it promoted the wetting of hydrophobic CNT walls with aqueous MPD solution so that CNTs were fully coated by polyamide during TFN fabrication as suggested in the literature [67]. In the absence of SDBS, detachment of polyamide layer in TFN membranes was observed several times. Therefore, SDBS was added to both TFC and TFN fabrication recipes so that synthesis conditions were identical and SDBS concentration of aqueous phase was determined based on the critical micelle concentration of the surfactant.

FTIR spectra of polysulfone support membrane and polyamide coated TFC membrane are shown in Figure 4.7. Region between 1400-1800 cm^{-1} where characteristic peaks of polyamide is observed may be examined. As seen, polysulfone characteristic peaks disappeared while C-N stretching (1510 cm^{-1}), amide C=O stretching (1620 cm^{-1}) and acid C=O stretching (1720 cm^{-1}) peaks appeared implying that polyamide layer was successfully synthesized [68].

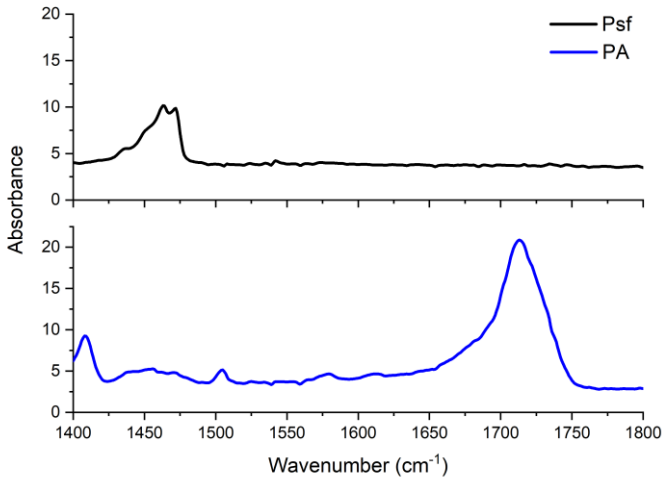

Figure 4.7: FTIR spectra of polysulfone support and polyamide coated TFC.

Another important factor affecting the formation of polyamide layer in TFN membranes is the dispersion of CNTs inside the polymeric matrix. Presence of functional groups (COOH or amino acids) and incubation with SDBS surfactant improved dispersion of CNTs in water. Besides, large CNT bundles and impurities were precipitated and removed via centrifugation. In the absence of this step, it was observed that CNTs piled as large aggregates as shown in Figure 4.8. These aggregates disrupted the integrity of polyamide layer and resulted in a significant decrease in salt rejection.

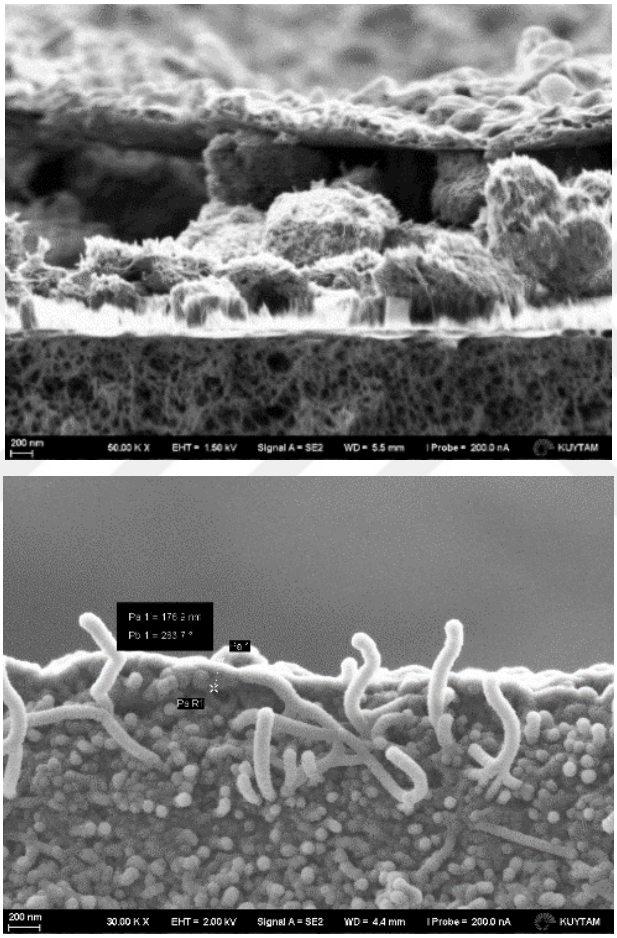

Figure 4.8: CNT aggregates (top picture) versus well-dispersed CNTs (bottom picture) in TFN membranes.

4.3 Effect of CNT Loading on the Structure and Performance of TFNs

TFN membranes containing COOH-CNT concentrations of 2.4, 1.2, 0.6 and 0.3 $x10^{13}/cm^2$ membrane were fabricated and characterized in order to determine optimum CNT loading. First, effect of CNT concentration on crosslinking ratio of polyamide layer was quantitatively determined by XPS analysis. For this purpose, C(1s), O (1s)

and N(1s) content of polyamide layer was analyzed and deconvolution of carbon and oxygen bonds was carried out for each membrane sample. An example XPS spectrum and chemical bond analysis was shown in Figure 4.9.

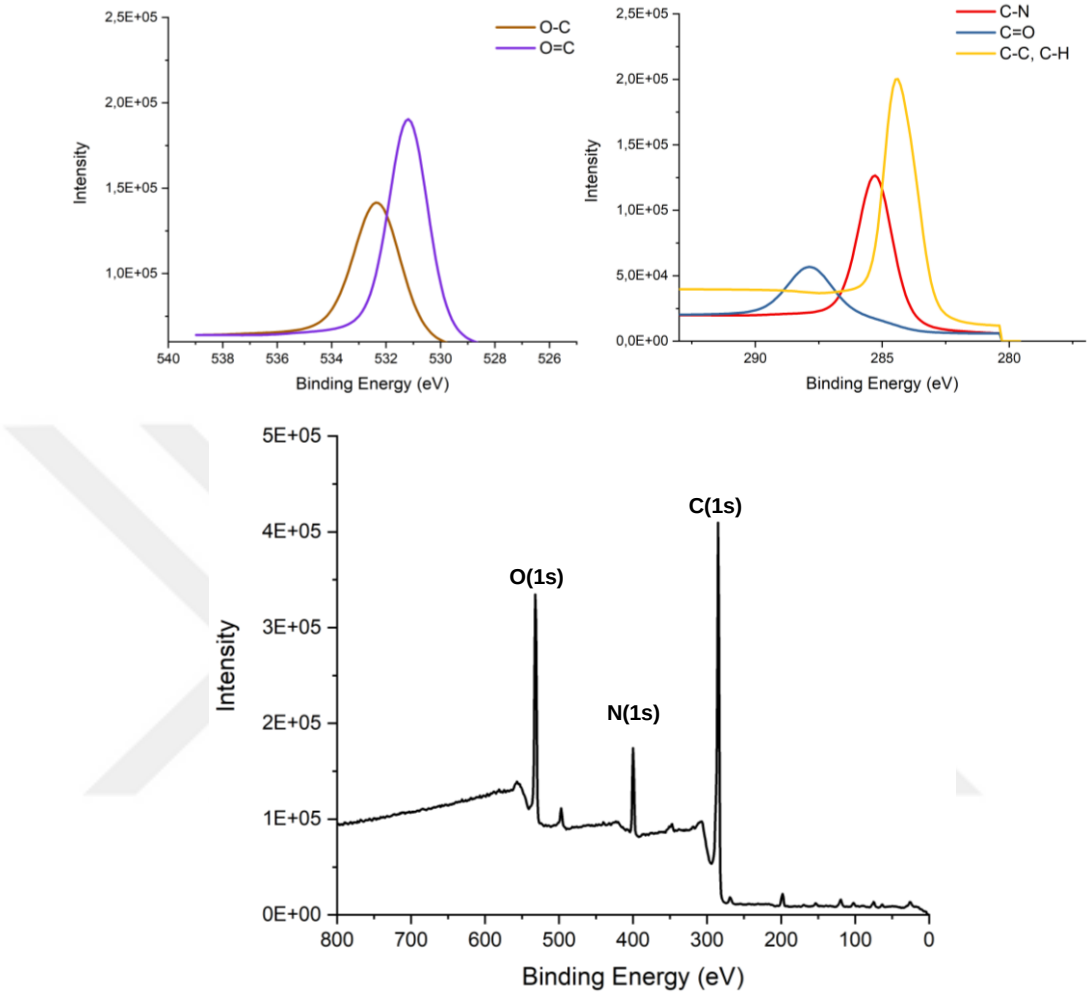

Figure 4.9: An example XPS spectrum and C(1s) and O(1s) deconvolution of polyamide.

Figure 4.10 shows crosslinked (m) and linear (n) polyamide chains formed as a result of interfacial polymerization (IP) of MPD and TMC monomers. Assuming that crosslinked part contributes 3m oxygen and 3m nitrogen while linear part contributes 4n oxygen and 2n nitrogen, m/n ratio and crosslinking ratio can be calculated from the equations (4.1) and (4.2) using experimental O/N ratio obtained from XPS. Theoretically, O/N ratio of a fully crosslinked membrane is 1 whereas a fully linear membrane has a O/N ratio of 2 [19]. Crosslinking ratio of TFC and TFN membranes prepared with different COOH-CNT loadings is presented in Table 4.2.

$$\frac{O}{N} = \frac{3m + 4n}{3m + 2n} \tag{4.1}$$

$$crosslinking\ ratio = \frac{m}{m+n} x100 \qquad (4.2)$$

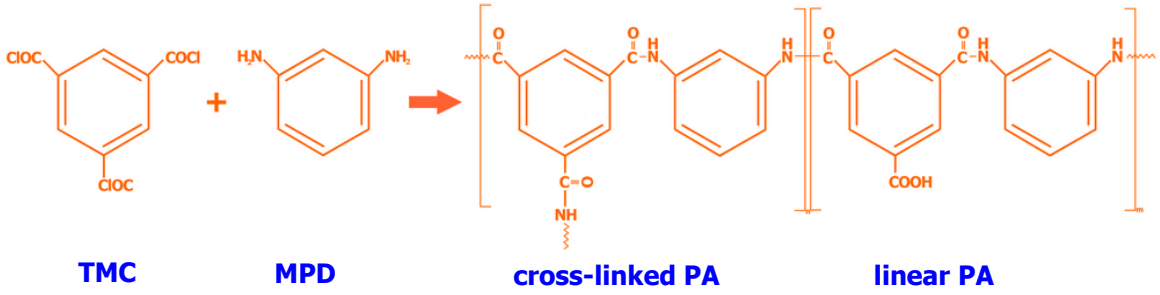

Figure 4.10: IP between TMC and MPD resulting in crosslinked and linear chains.

Table 4.2: Crosslinking ratio of polyamide layers prepared with different COOH-CNT loadings.

# of CNTs x10^{-13} (/cm^2membrane)	O(1s) %	N(1s) %	O/N ratio	Crosslinking ratio
2.4 x10^{13}	12.4	11.6	1.12	82.5
1.2 x10^{13}	15.4	8.72	1.96	2.49
0.6 x10^{13}	10.2	8.86	1.49	41.4
0.3 x10^{13}	11.4	9.16	1.40	49.7
0.0 x10^{13}	11.5	8.18	1.40	50.0

The TFN membranes prepared with 0.3 x10^{13}/cm^2 CNT loading resulted in a crosslinking ratio very close to that of plain polyamide while 0.6 x10^{13}/cm^2 loading resulted in a slight decrease. Interestingly, highest CNT loading resulted in the highest crosslinking ratio implying that excess CNTs might form a second layer between support layer and polyamide instead of vertically aligned through the support pores. This additional layer might lead to formation of highly crosslinked polyamide on top of CNT layer. On the contrary, 1.2 x10^{13}/cm^2 CNT loading resulted in a dominantly linear polyamide layer indicating that this CNT concentration might disrupt crosslinking of the polymer.

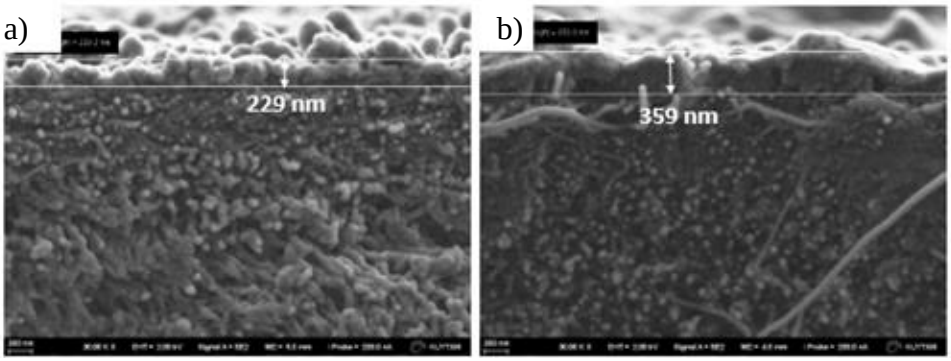

Figure 4.11: SEM cross-sections of TFNs with a) 2.4x10^{13}/cm^2, b) 1.2x10^{13}/cm^2 CNT.

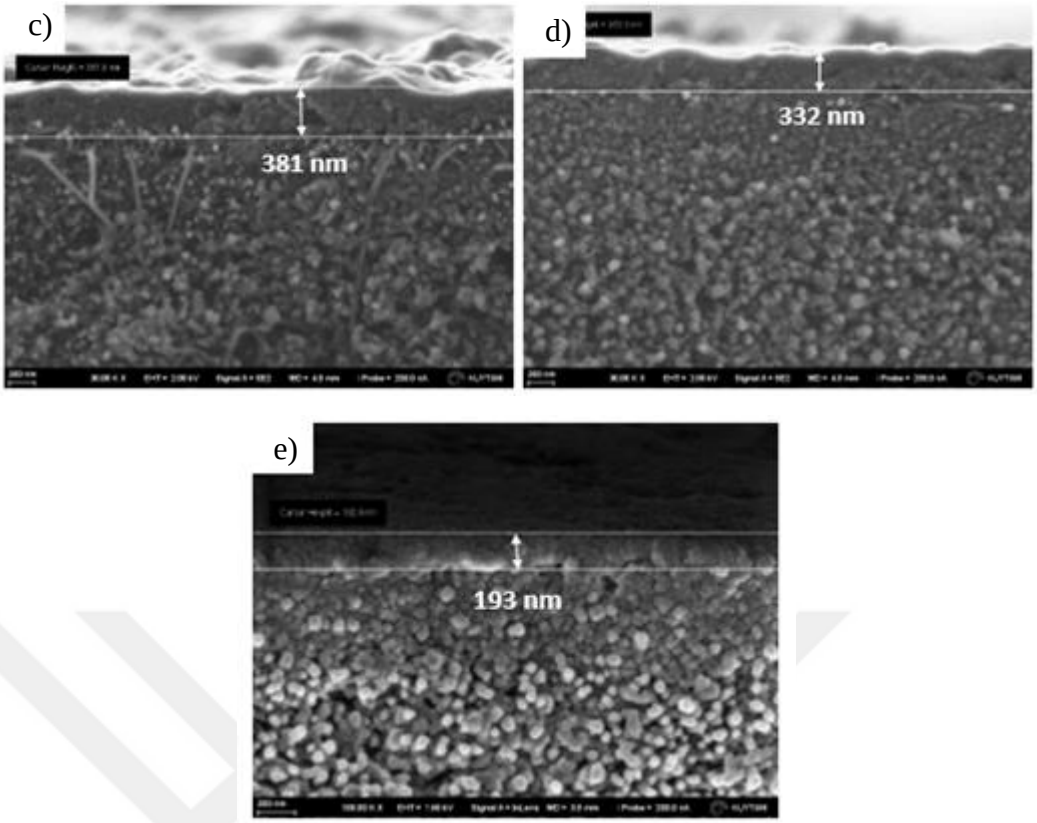

Figure 4.11 (continued): SEM cross-sections of TFNs prepared with c) $0.6x10^{13}/cm^2$, d) $0.3x10^{13}/cm^2$ CNT and e) TFC.

Morphology of the membranes has significant effect on the flow dynamics of water and fouling properties. In this study, SEM and AFM were used for morphological characterization. Figure 4.11 shows SEM cross-sections of TFC and TFN membranes prepared with different CNT loadings. Polyamide thickness of TFC was measured approximately 200 nm while polyamide thickness of TFN membranes varied between 230-380 nm. CNTs aligned through the pores of support membranes possibly led to narrowing of these pores and limited the diffusion of MPD during interfacial polymerization. Increased thickness of the TFN membranes might have resulted from this effect. It is also observed that crosslinking ratio and thickness of the polyamide are not directly related and both may impact the overall water flux. In addition, SEM images taken from different regions of TFN membrane prepared with CNT loading of $1.2x10^{13}/cm^2$ presented in Figure 4.12. Cross-section images clearly show the randomly aligned CNT bundles hanging from polyamide layer. Since CNTs used in experiments have an average diameter of 1 nm, these tube-like structures were considered as CNT bundles.

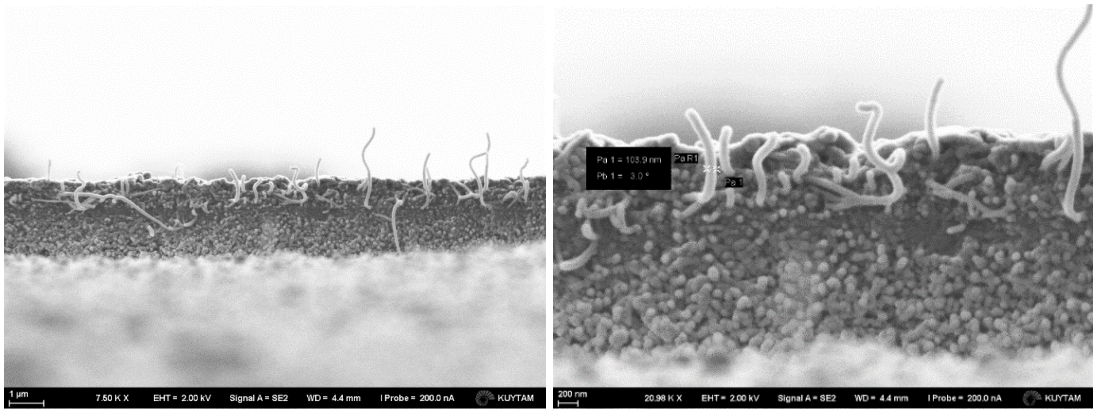

Figure 4.12: SEM cross-sections showing randomly aligned CNT inside polyamide.

Surface morphologies of TFC and TFN membranes were evaluated via SEM and AFM as shown in Figure 4.13. Polyamide surface prepared with the highest CNT loading is very similar to surface of plain TFC polyamide corresponding with XPS results. Excess CNT loading interfered with partial alignment and led to formation of a CNT layer underneath polyamide. When surface of other TFN membranes are examined, no significant change in surface morphology was observed except that TFN membrane prepared with $1.2x10^{13}/cm^2$ resulted in a less homogeneous surface with high surface features.

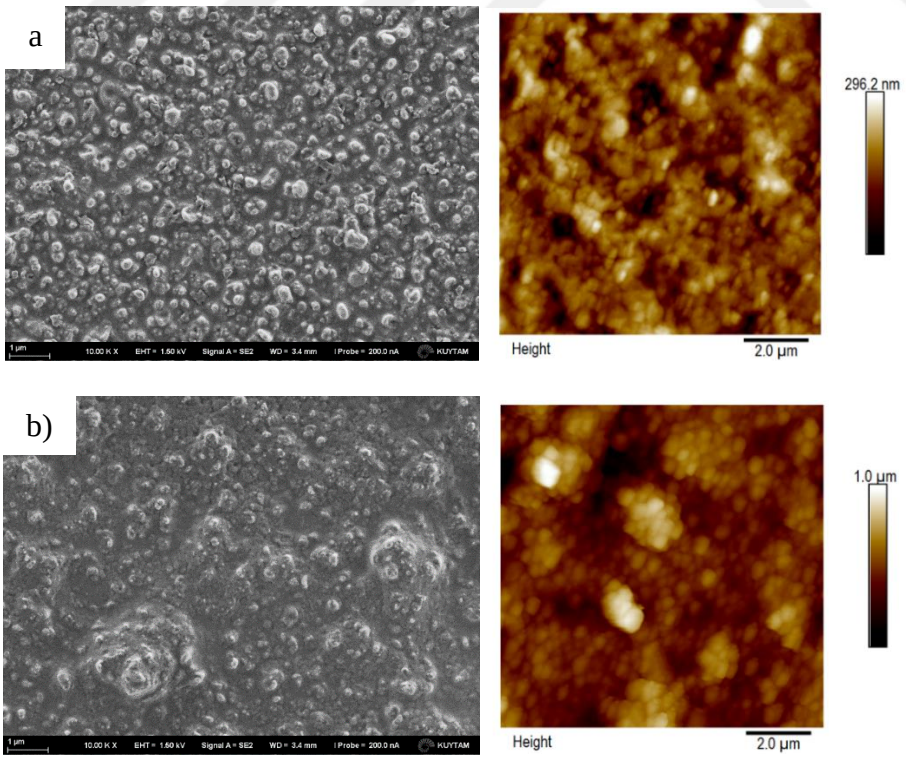

Figure 4.13: SEM and AFM surface images of TFNs prepared with a) $2.4x10^{13}/cm^2$, b) $1.2x10^{13}/cm^2$.

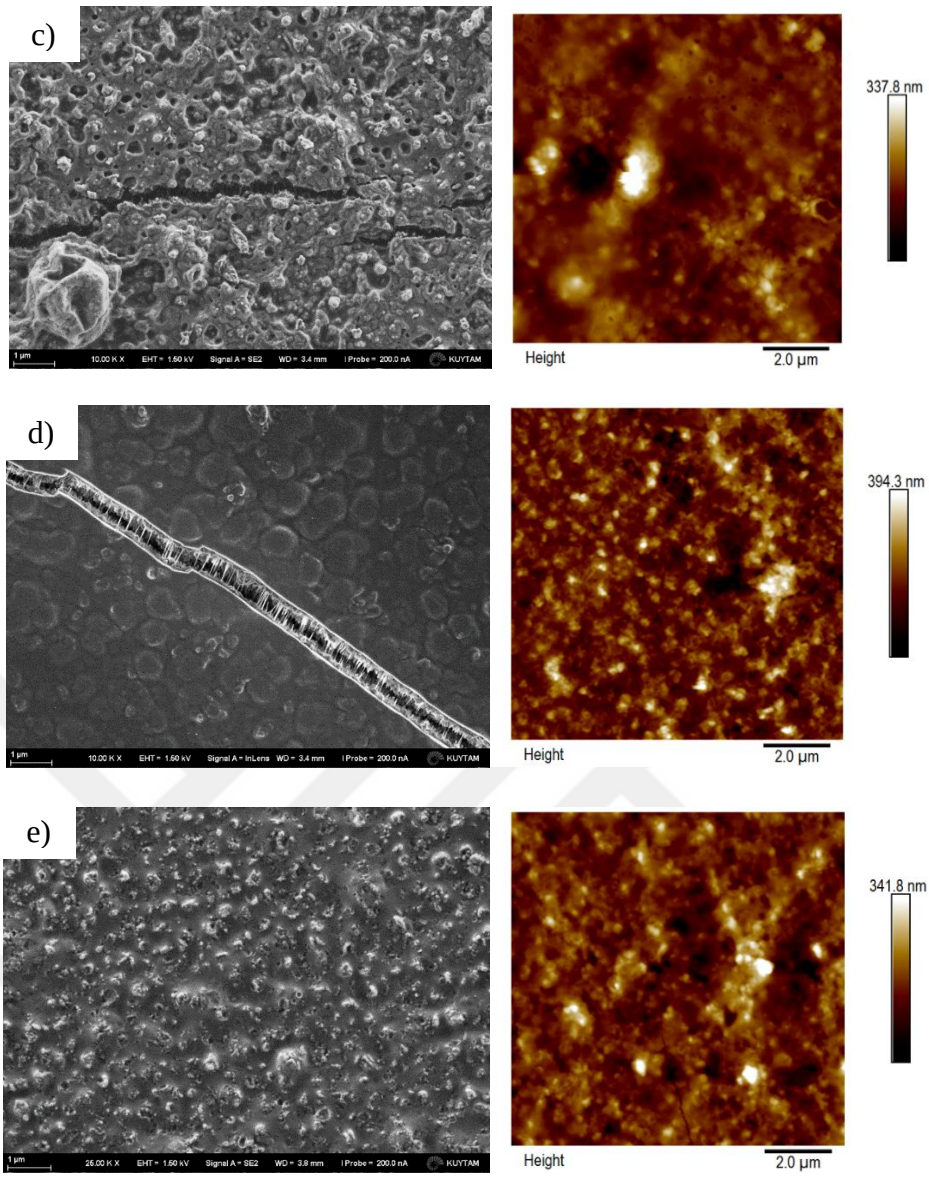

Figure 4.13 (continued): SEM and AFM surface images of TFNs prepared with c) $0.6x10^{13}/cm^2$, d) $0.3x10^{13}/cm^2$ CNT loading, e) TFC (Scale bar is 1µm).

In addition, fractures were observed in the TFN surfaces containing 0.6 and 0.3 $x10^{13}/cm^2$ CNT as shown in Figure 4.13 c and d. Considering high salt rejection of these membranes, fractures were not evaluated as polyamide defects and they were attributed to high vacuum applied during SEM analysis. Figure 4.14 shows CNTs become visible through the fractures in detail. Diameter of different CNT bundles were measured between 7-33 nm.

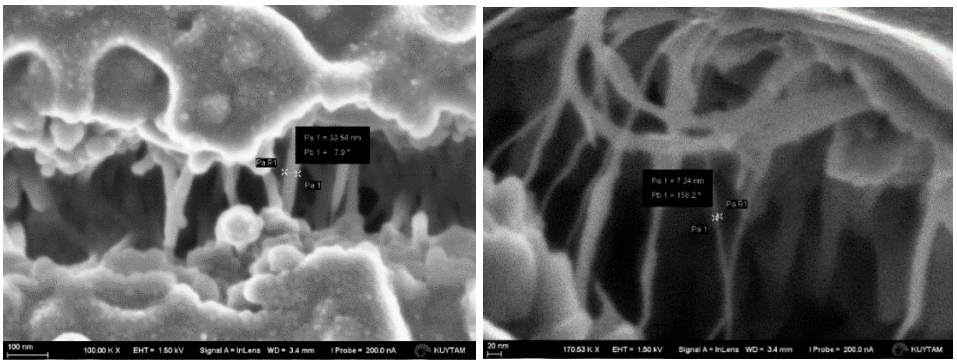

Figure 4.14: CNT bundles seen through surface fractures in TFN surfaces.

Alignment of CNTs inside the polymeric matrix is very important to fully exploit fast water transport properties. Vertically aligned CNTs are desirable since they form additional channels for passage of water. However, no electric or magnetic field was applied during membrane fabrication in this study and partial alignment of CNTs relied on vacuum filtration. Figure 4.15 depicts schematics of TFN fabrication steps and how CNTs might be aligned during the process. As shown, it was predicted that majority of CNTs randomly aligned and this prediction was confirmed by SEM cross-section images.

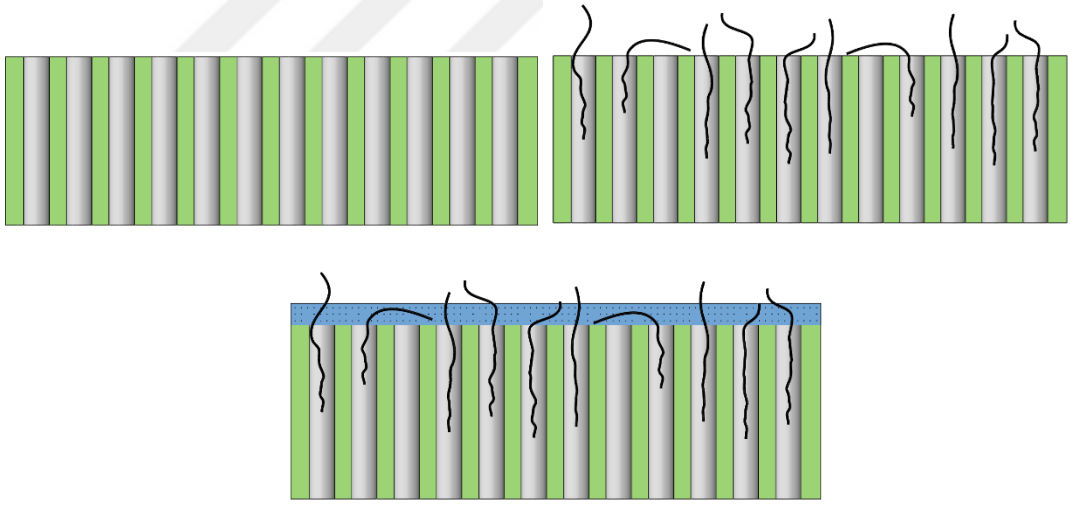

Figure 4.15: Schematic representation of support layer, random alignment of CNTs through support pores and coating with polyamide layer, respectively.

Polarized Raman spectroscopy was employed to make quantitative evaluation of CNT alignment inside the polymeric matrix. Depending of their alignment, molecular vibrations of CNTs interact differently with polarization of Raman laser. When polarization is parallel to CNT axis (0° or 180° polarization) maximum peak intensity was observed whereas perpendicular polarization (90° polarization) results in the

minimum peak intensity [69]. Figure 4.16 shows the Raman spectra of a TFN membrane surface prepared with 1.2 x10^{13}/cm^2 loading at parallel and perpendicular polarizations. Peak intensity at parallel polarization interacting with vertically aligned CNTs is greater than the peak intensity of perpendicular polarization interacting with horizontal CNTs indicating that vertical alignment dominated. However, low CNT concentration resulted in completely random alignment.

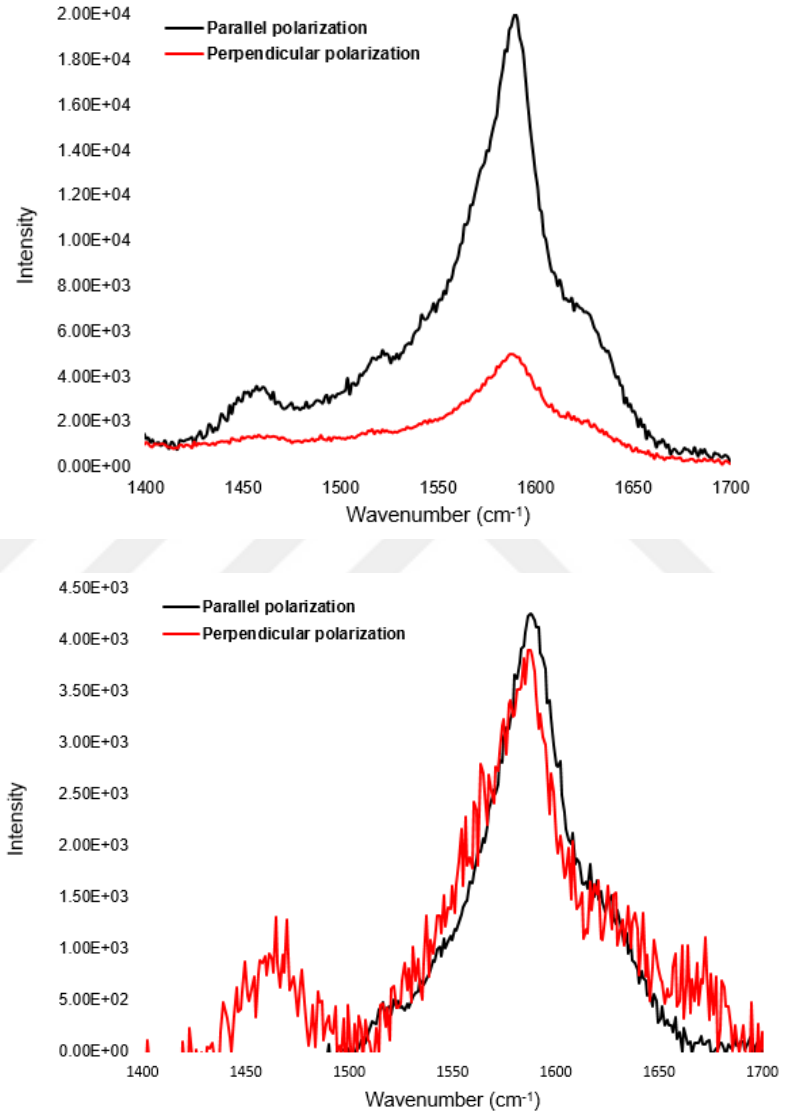

Figure 4.16: Polarized Raman spectra belonging to TFN membranes prepared with 1.2 and 0.3 x10^{13}/cm^2 COOH-CNT loadings, respectively.

Surface roughness obtained from AFM and water contact angle data is presented in Figure 4.17. Measurements were taken from three different region of the sample for each membrane and standard deviation was indicated by error bars. Incorporation of hydrophobic CNTs significantly decreased the hydrophilicity of membrane surface as indicated by high contact angle values. Hydrophobicity of TFN membrane with

highest CNT loading might be explained by high crosslinking ratio resulting in low pendant carboxylic acid concentration in polyamide chains since CNTs were thought to be located underneath the polyamide. Roughness did not correlate with CNT concentration but usually higher in TFNs compared to TFC. It was noted that roughness at $1.2x10^{13}/cm^2$ CNT loading is significantly higher, indicating a les homogeneous polyamide surface was obtained.

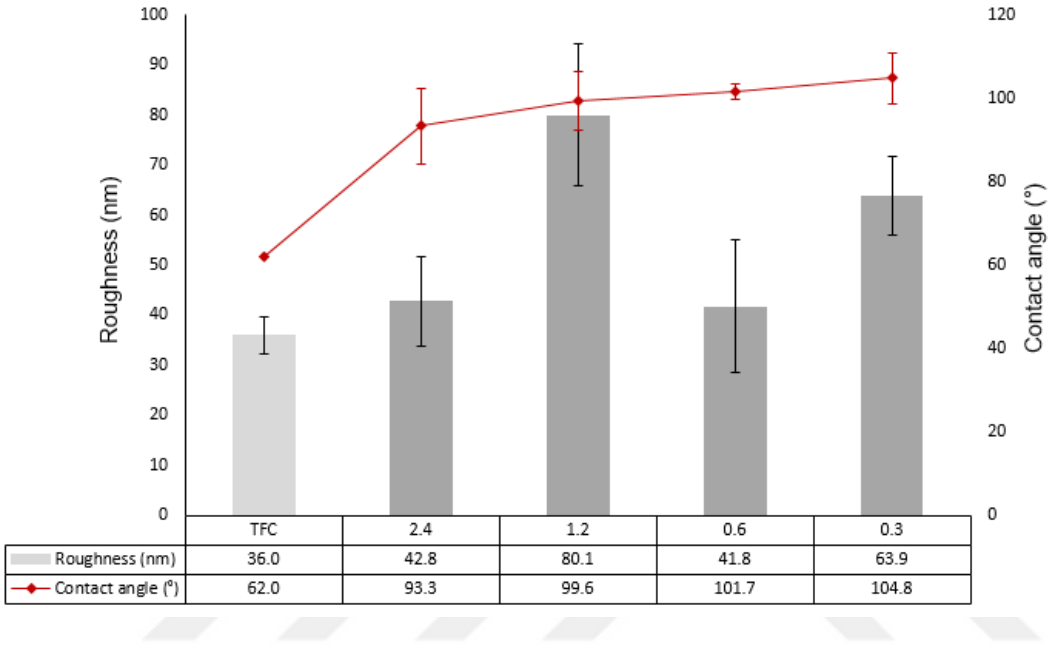

Figure 4.17: Surface roughness and water contact angle of TFC and TFN membranes (COOH-CNT loading is given as $x10^{-13}/cm^2$ membrane)

Table 4.3: Salt rejection and water flux of TFC and TFN membranes prepared with different COOH-CNT loadings.

Membrane code	CNT loading $x10^{-13}/cm^2$		Salt rejection, %	Water flux, LMH
TFC 1	0.0		98.3	28.5
TFC 2	0.0		97.8	15.1
TFC 3	0.0		97.3	19.8
		avg.	**97.8**	**21.1**
		std.	0.5	6.8
TFN 1	2.4		95.3	18.1
TFN 2	2.4		96.3	34.1
TFN 3	2.4		94.0	12.2
		avg.	**95.2**	**21.5**
		std.	1.2	11.3
TFN 4	1.2		96.9	25.9
TFN 5	1.2		93.3	7.3
TFN 6	1.2		93.6	16.8
		avg.	**94.6**	**16.7**
		std.	2.0	9.3

Table 4.3 (continued): Salt rejection and water flux of TFC and TFN membranes prepared with different COOH-CNT loadings.

Membrane code	CNT loading $x10^{-13}/cm^2$	Salt rejection, %	Water flux, LMH
TFN 7	0.6	98.2	33.3
TFN 8	0.6	98.4	17.6
TFN 9	0.6	98.3	14.2
	avg.	**98.3**	**24.0**
	std.	0.1	8.2
TFN 10	0.3	96.9	14.1
TFN 11	0.3	97.1	11.1
TFN 12	0.3	97.9	19.6
	avg.	**97.3**	**14.9**
	std.	0.5	4.3

Water flux and salt rejection data of TFC and TFN membranes is presented in Table 4.3. For every loading, membranes were prepared as three replicates under identical synthesis conditions. Graphical representation of average salt rejection and water flux values are presented in Figure 4.18. Standard deviations were also indicated by error bars. CNT loadings of 2.4 and 1.2 $x10^{13}/cm^2$ have negative effect on overall separation performance of membranes. They resulted in low salt rejection compared to TFC and no improvement in water flux was observed. Besides, variation in both salt rejection and water flux among replicates suggests high probability of defect formation. As seen, 0.3 $x10^{13}/cm^2$ CNT loading retained salt rejection but decreased water flux compared to TFC with a lower variation among replicates. In this case, decrease in water flux might be attributed to hydrophobicity of membrane surface as well as random alignment. Lastly, 0.6 $x10^{13}/cm^2$ CNT loading improved both salt rejection and water flux and determined as the optimum CNT loading.

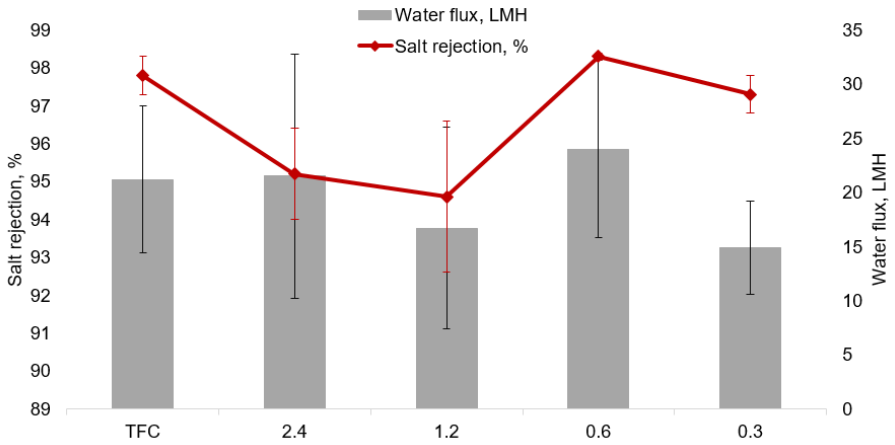

Figure 4.18: Average salt rejection and water flux of TFC and TFN membranes with different CNT loadings. (Error bars represent standard deviation.)

4.4 Effect of Functional Group on the Structure and Performance of TFNs

To investigate the effect of functional group, TFN membranes containing Asn-CNT and ACA-CNT were prepared at CNT loading of 0.6 x10^{13}/cm^2 which was determined as the optimum loading. The crosslinking ratios of plain polyamide and polyamides containing COOH, Asn and ACA functionalized CNTs determined from XPS analysis are presented in Table 4.4. While the Asn amino acid slightly increased the crosslinking ratio of polyamide chains with respect to that of plain poliamide, ACA amino acid had a negative effect on crosslinking possibly due to its bulky structure.

Table 4.4: Crosslinking ratio of polyamide layers prepared with different functional groups.

CNT type	O(1s) %	N(1s) %	O/N ratio	Crosslinking ratio
-	11.5	8.18	1.40	50.0
COOH-CNT	10.2	8.86	1.49	41.4
Asn-CNT	13.0	9.49	1.37	53.3
ACA-CNT	15.0	8.56	1.75	18.2

Cross-sectional morphology of TFN membranes containing Asn and ACA functionalized CNTs are in-line with the crosslinking analysis. Figure 4.19 shows that Asn-CNT incorporation resulted in a thinner polyamide layer compared to TFN prepared with COOH-CNT, whereas ACA-CNT led to formation of the thickest polyamide layer among all membranes.

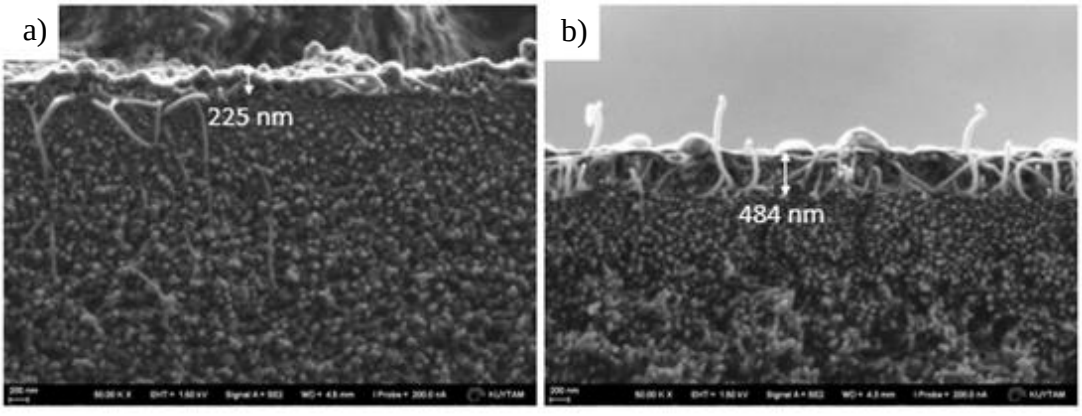

Figure 4.19: SEM cross-section of TFN membranes prepared with a) Asn-CNT and b) ACA-CNT. (CNT loading is 0.6 x10^{13}/cm^2)

Figure 4.20 shows surface images obtained by SEM and AFM. Asn-COOH resulted in a homogenous polyamide surface and morphology is similar to TFC membrane. On

the other hand, ACA-CNTs caused forming ring-like structures on the surface. Similar structures observed by Cadotte et. al is attributed to presence of excess carboxyl groups which may cause swelling of the polymer during interfacial polymerization [15].

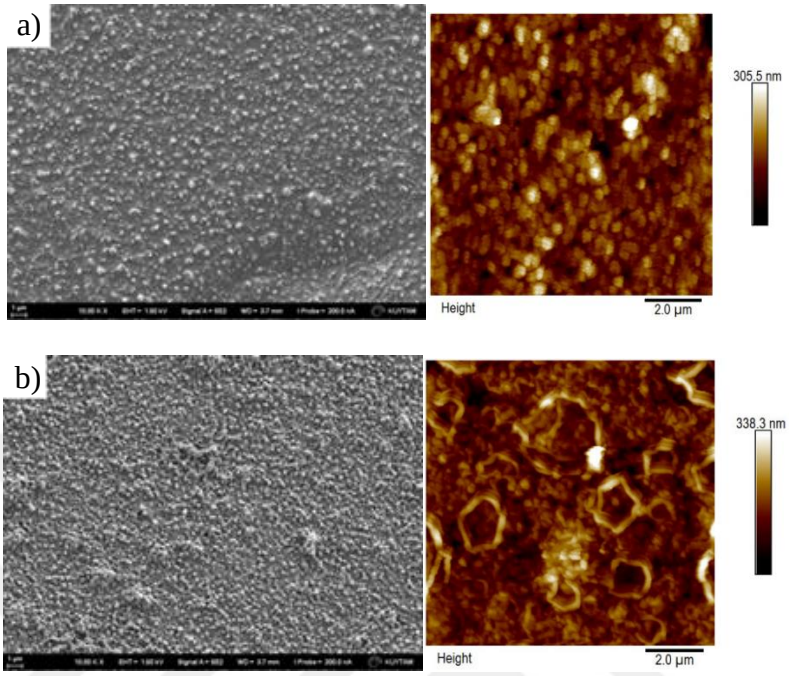

Figure 4.20: Surface morphologies of membranes prepared with a) Asn-CNT, b) ACA-CNT obtained by SEM and AFM. (SEM scale bar is 1 µm.)

Effect of Asn amino acid on CNT alignment was examined via Polarized Raman spectroscopy. Figure 4.21 shows the Raman spectra of two replicate TFN membranes containing Asn-CNTs at parallel and perpendicular polarizations. As discussed in section 4.3, peak intensity at parallel polarization is considerably higher than peak intensity at perpendicular polarization for both membranes implying that majority of CNTs were vertically aligned.

Roughness obtained from AFM measurements and water contact angle data are presented in Figure 4.22. Measurements were taken from three different region of the sample for each membrane and standard deviation was indicated by error bars. Roughness of TFC and other three TFN membranes prepared with different functional groups are very similar. On the other hand, it is seen that asparagine significantly improved surface hydrophilicity. While TFN membranes prepared with COOH-CNTs are hydrophobic, use of asparagine as functional group resulted in very similar contact angle with TFC. There might be two reasons for that: First, asparagine molecule can contribute favorable interactions with water due to its high hydrogen bonding capacity.

Second, asparagine may improve dispersion and vertical alignment resulting in a decreased expression of hydrophobic CNT walls on the membrane surface. ACA functional group may be also considered to provide some hydrophilicity improvement.

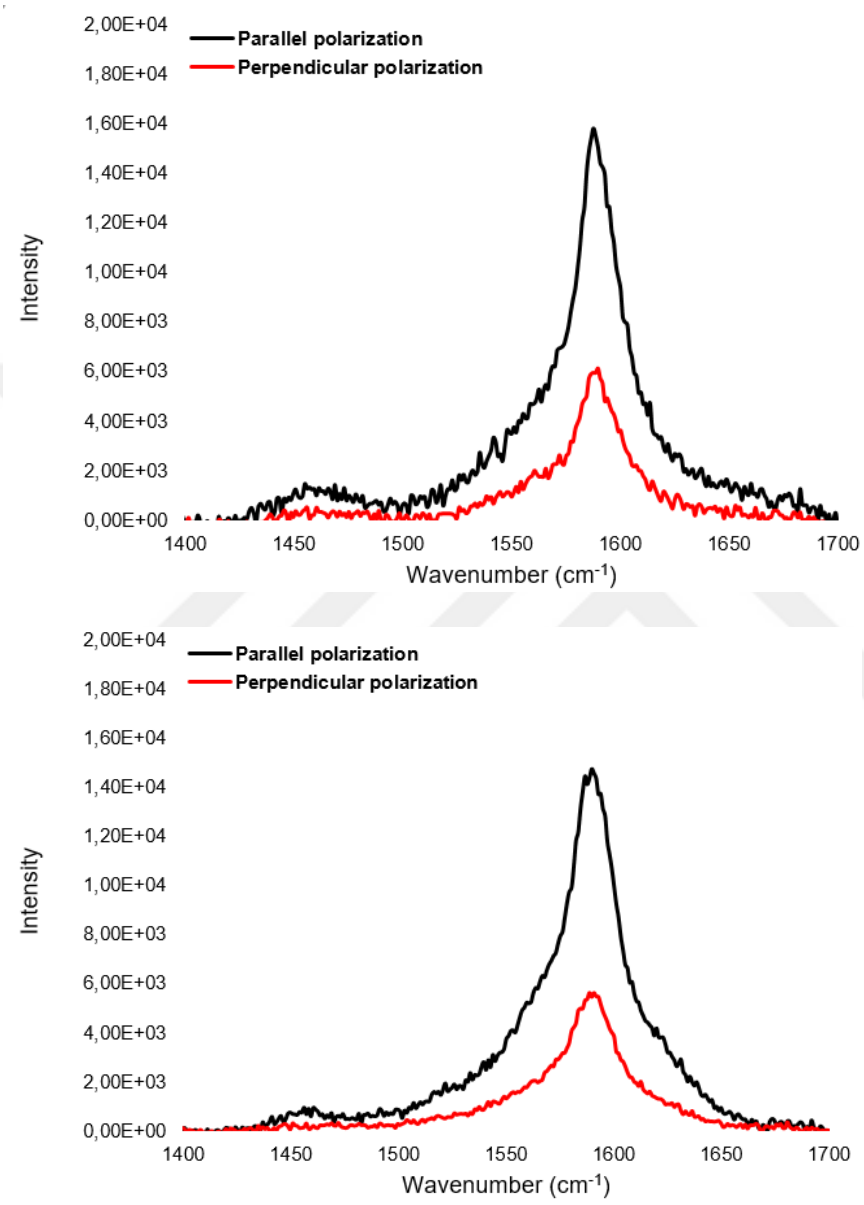

Figure 4.21: Polarized Raman spectra of two replicate Asn-CNT containing TFNs.

Lastly, separation performance of TFC and TFN membranes prepared with COOH, Asn and ACA functionalized CNTs is presented in Table 4.5 as well as graphical summary in Figure 4.23. Again, membranes containing different functional groups were prepared as three replicates under identical synthesis conditions. It is seen that use of asparagine improved water flux compared to both TFC and TFN containing

COOH-CNTs while average salt rejection is 98.3%. In addition, low variability among replicates shows that reproducibility is also improved. It may be concluded that asparagine functionalized carbon nanotubes have more favorable interactions with the polyamide, producing a defect-free, thin and highly crosslinked polyamide layer. High hydrogen bonding capacity of asparagine contributed to surface hydrophilicty and water flux as indicated by water contact angle and performance results.

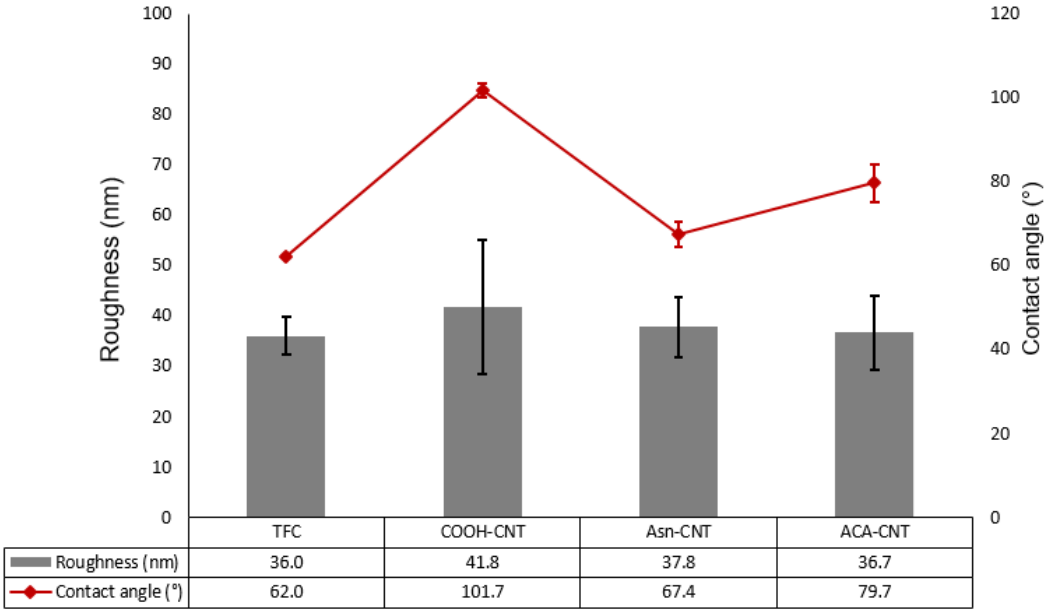

	TFC	COOH-CNT	Asn-CNT	ACA-CNT
Roughness (nm)	36.0	41.8	37.8	36.7
Contact angle (°)	62.0	101.7	67.4	79.7

Figure 4.22: Roughness and water contact angle for TFC and TFN membranes with different functional groups. (CNT loading is 0.6 x10^{13}/cm^2)

Another effect of asparagine leading to improved hydrophilicty and water permeability is thought to be its contribution to vertical alignment of CNTs as indicated by Polarized Raman analysis. For TFN membranes prepared with Asn-CNTs, no significant improvement was observed in terms of ion rejection compared to COOH-CNTs. On the other hand, ACA amino acid having a larger molecular size did not create the expected steric hindrance. Bulk stucture of the molecule may interfere with the polymerization reaction and crosslinking of polyamide chains resulting in pin-hole defects and reduced salt rejection. SEM and AFM surface morphologies as well as crosslinking ratio obtained from XPS analysis support this theory. and it is evident that ACA does not provide any improvement in terms of both water flux and salt rejection.

Table 4.5: Salt rejection and water flux of TFC and TFN membranes prepared with different functional groups.

Membrane code	CNT type	Salt rejection, %	Water flux, LMH
TFC 1	-	98.3	28.5
TFC 2	-	97.8	15.1
TFC 3	-	97.3	19.8
	avg.	**97.8**	**21.1**
	std.	0.5	6.8
TFN 7	COOH-CNT	98.2	33.3
TFN 8	COOH-CNT	98.4	17.6
TFN 9	COOH-CNT	98.3	14.2
	avg.	**98.3**	**24.0**
	std.	0.1	8.2
TFN 13	Asn-CNT	98.0	32.9
TFN 14	Asn-CNT	97.5	19.0
TFN 15	Asn-CNT	98.5	25.4
	avg.	**98.3**	**26.5**
	std.	0.3	5.9
TFN 16	ACA-CNT	98.0	20.1
TFN 17	ACA-CNT	95.9	23.5
TFN 18	ACA-CNT	97.6	21.3
	avg.	**97.2**	**21.6**
	std.	1.1	1.7

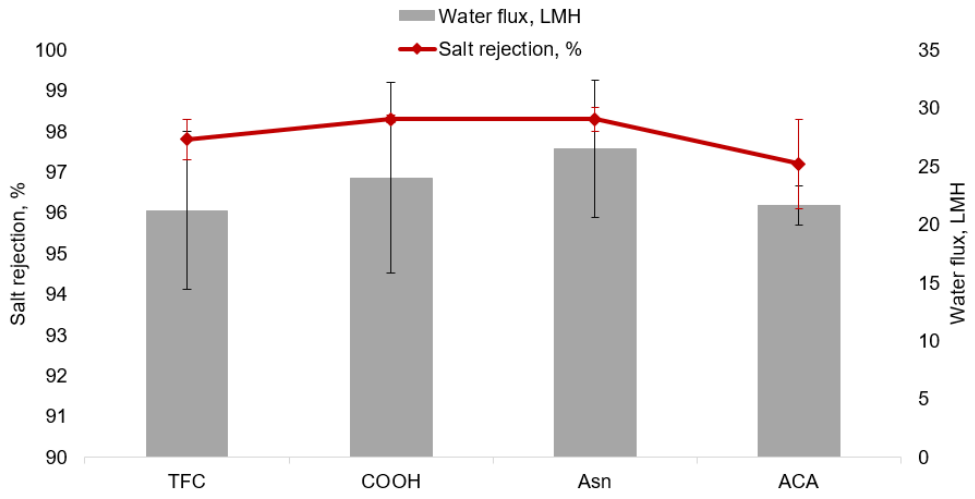

Figure 4.23: Average salt rejection and water flux of TFC and TFN membranes containing different functional groups at CNT loading of 0.6 x10^{13}/cm^2. (Error bars represent standard deviation.)

5. CONCLUSIONS AND RECOMMENDATIONS

In this study, effect of amino acid functionalized carbon nanotubes on the structure, morphology and separation performance of TFN membranes was investigated. Inspried by structure of biological aquaporin channels, asparagine (Asn) amino acid was used as functional group in order to improve water permeability and salt rejection. The second amino acid, 8-aminocaprylic acid (ACA) was used due to its bulky structure in order to create steric hindrance for ions by narrowing the entrance of CNTs.

Amino acid functionalization of carboxylated CNTs (COOH-CNTs) was carried out via carbodiimide mediated reaction. Replacement of COOH groups with amino acids was confirmed by TGA and XPS. Based on the atomic composition data obtained from XPS, conversion ratio of carboxyl groups to Asn and ACA was calculated as 7.15% and 9.72%, respectively. Raman spectrometry analysis showed that amino acid functionalization caused a slight decrease in G/D ratio; however, stability of CNTs was acceptable.

XPS, SEM, AFM and polarized Raman analyses of TFN membranes prepared with different COOH-CNT loadings showed that concentration of CNT significantly affects dynamics of interfacial polymerization reaction. Crosslinking, surface morphology and thickness of polyamide layer were found to be related to CNT loading. This effect may be attributed to different dispersion and alignment behaviors of CNTs at different loadings. Furthermore, COOH-CNT incorporation significantly decreased surface hydrophilicity suggesting that hydrophobic walls of CNTs were expressed at or near the membrane surface. Based on salt rejection and water flux as well as structural and morphological properties, optimum CNT loading was determined as 0.6×10^{13} CNTs/cm^2.

At this optimum loading, Asn-CNTs allowed the formation of a thin and homogeneous polyamide layer having similar morphology with TFC. Therefore, it was concluded that Asn did not negatively affect crosslinking of polyamide. In addition, Asn considerably contributed to the surface hydrophilicity compared to carboxyl groups.

Due to its high hydrogen bonding capacity and favorable interactions with water molecules, effect of hydrophobic CNT walls was compensated. Use of asparagine as functional group improved average water flux from 21.1 to 26.5 LMH and average salt rejection from 97.8% to 98.3% compared to TFC membranes. On the other hand, ACA functionalization caused formation of a morphologically different polyamide layer. It was thought that bulk ACA molecules interfered with crosslinking of polyamide chains, producing more linear and thick polyamide layer having pin-hole defects. Bulk structure of the molecule did not provide the expected steric hindrance and caused a slight decrease in both water flux and salt rejection.

Both SEM and polarized Raman results indicated that vacuum filtration was not adequate to provide full vertical alignment of CNTs and alignment inside the polymeric matrix was generally random. In order to fully exploit fast water transport properties of CNTs, vertical alignment may be promoted by electric field which needs to be applied during interfacial polymerization process.

REFERENCES

[1] **WWAP (United Nations World Water Assessment).** (2017). *The United Nations World Water Development Report 2017: Wastewater, The Untapped Resource*. Paris: UNESCO.

[2] **WWAP (United Nations World Water Assessment).** (2018). *The United Nations World Water Development Report 2018: Nature-Based Solutions for Water*. Paris: UNESCO.

[3] **Cohen, Y., Semiat, R., & Rahardianto, A.** (2017). A perspective on reverse osmosis water desalination: Quest for sustainability. *AIChE J.*, *63* (6), 1771–1784.

[4] **Amy, G., Ghaffour, N., Li, Z., Francis, L., Linares, R. V., Missimer, T., & Lattemann, S.** (2017). Membrane-based seawater desalination: Present and future prospects. *Desalination*, *401*, 6–21.

[5] **Werber, J. R., Osuji, C. O., & Elimelech, M.** (2016). Materials for next-generation desalination and water purification membranes. *Nat. Rev. Mater.*, *1*, 1-15.

[6] **Yin J., and Deng, B.** (2015) Polymer-matrix nanocomposite membranes for water treatment. *J. Memb. Sci.*, *479*, 256–275.

[7] **Yang, Z., Ma, X. H., Tang, & C. Y.** (2018) Recent development of novel membranes for desalination. *Desalination*, *434*, 37–59.

[8] **Noy, A., Park, H. G., Fornasiero, F., Holt, J. K., Grigoropoulos, C. P., & Bakajin, O.** (2007) Nanofluidics in carbon nanotubes Extremely high aspect ratios , molecularly smooth hydrophobic graphitic. *Nanotoday*, *2* (6) 22–29.

[9] **Hummer, G., Rasaiah, J. C., & Noworyta, J. P.** (2001) Water conduction through the hydrophobic channel of a carbon nanotube. *Nature*, *414*, 188–190.

[10] **Agre, P.** (2006). The aquaporin water channels. *Proc. Am. Thorac. Soc.*, *3* (1), 5-13.

[11] **Barboiu, M.** (2016) Artificial water channels: Incipient innovative developments. *Chem. Commun.*, *52* (33), 5657–5665.

[12] **Baker, R. W.** (2004). *Membrane Technology and Applications*, 2nd ed. New

York: Wiley.

[13] **Loeb, S. and Sourirajan, S.** (1963) Sea Water Demineralization by Means of an Osmotic Membrane. *Saline Water Conversion II,* 117–132.

[14] **Lonsdale, H. K.** (1987). The evolution of ultrathin synthetic membranes. *J. Memb. Sci.*, *33* (2), 121–136.

[15] **Cadotte, J. E., King, R. S., Majerle, R. J., & Petersen, R. J.** (1981) Interfacial Synthesis in the Preparation of Reverse Osmosis Membranes. *J. Macromol. Sci. Part A - Chem.*, *15* (5), 727–755.

[16] **Lau, W. J., Ismail, A. F., Misdan, N., & Kassim, M. A.** (2012). A recent progress in thin film composite membrane: A review. *Desalination*, *287*, 190–199.

[17] **Ghosh, A. K., Jeong, B. H., Huang, X., & Hoek, E. M. V.** (2008). Impacts of reaction and curing conditions on polyamide composite reverse osmosis membrane properties. *J. Memb. Sci.*, *311* (1-2) 34–45.

[18] **Khorshidi, B., Thundat, T., Fleck, B. A., & Sadrzadeh, M.** (2016). A novel approach toward fabrication of high performance thin film composite polyamide membranes. *Sci. Rep.*, *6*, 1–10.

[19] **Xie, W., Geise, G. M., Freeman, B. D., Lee, H. S., Byun, G., & McGrath, J. E.** (2012). Polyamide interfacial composite membranes prepared from m-phenylene diamine, trimesoyl chloride and a new disulfonated diamine. *J. Memb. Sci.*, *403–404*, 152–161.

[20] **Yong, Z., Sanchuan, Y., Meihong, L., & Congjie, G.** (2006). Polyamide thin film composite membrane prepared from m-phenylenediamine and m-phenylenediamine-5-sulfonic acid. *J. Memb. Sci.*, *270* (1–2), 162–168.

[21] **Kong, C., Kanezashi, M., Yamomoto, T., Shintani, T., & Tsuru, T.** (2010). Controlled synthesis of high performance polyamide membrane with thin dense layer for water desalination. *J. Memb. Sci.*, *362* (1–2), 76–80.

[22] **Chan, W., Chen, H., Surapathi, A., Taylor, M. G., Shao, X, Marand, E & Al, C. E. T.** (2013). Zwitterion Functionalized Carbon Nanotube / Polyamide Nanocomposite. *ACS Nano*, *6*, 5308–5319.

[23] **Inukai, S., Cruz-Silva, R., Ortiz-Medina, J., Morelos-Gomez, A., Takeuchi, K., Hayashi, T., Tanioka, A., Araki, T., Tejima, S, Noguchi, T., Terrones, M., & Endo, M.** (2015). High-performance multi-functional reverse osmosis membranes obtained by carbon nanotube·polyamide nanocomposite. *Sci. Rep.*, *5*, 1–10.

[24] **DOW FILMTEC Membranes**, "SW30HR-380." Midland, Michigan U.S.A. 48674.

[25] **Hydranautics Corporate,** "SWC5-LD." 401 Jones Road, Oceanside, CA, U.S.A. 92058.

[26] **TORAY Membrane USA,** "TM840M-1760." 13435 Danielson Street, Poway CA, U.S.A. 92064.

[27] **Park, H. B., Kamcev, J., Robeson, L. M., Elimelech, M., & Freeman, B. D.** (2017) Maximizing the right stuff: The trade-off between membrane permeability and selectivity. *Science, 356,* 1138–1148.

[28] **Werber, J. R., Deshmukh, A., & Elimelech, M.** (2016). The Critical Need for Increased Selectivity, Not Increased Water Permeability, for Desalination Membranes. *Environ. Sci. Technol. Lett., 3* (4), 112–120.

[29] **Jeong, B. H., Hoek, E. M. V., Yan, Y., Subramani, A., Huang, X, Hurwitz, G., Ghosh, A. K., & Jawor, A.** (2007) Interfacial polymerization of thin film nanocomposites: A new concept for reverse osmosis membranes. *J. Memb. Sci., 294* (1–2), 1–7.

[30] **Lau, W. J., Gray, S., Matsuura, T., Emadzadeh, D., Paul-Chen, J., & Ismail, A. F.** (2015) A review on polyamide thin film nanocomposite (TFN) membranes: History, applications, challenges and approaches. *Water Res., 80,* 306–324.

[31] **Chan, W. F., Marand, E & Martin, S. M.** (2016) Novel zwitterion functionalized carbon nanotube nanocomposite membranes for improved RO performance and surface anti-biofouling resistance. *J. Memb. Sci., 509,* 125–137.

[32] **Chae, H. R., Lee, J., Lee, C. H., Kim, I. C., & Park, P. K.** (2015) Graphene oxide-embedded thin-film composite reverse osmosis membrane with high flux, anti-biofouling, and chlorine resistance. *J. Memb. Sci., 483,* 128–135.

[33] **De Lannoy, C. F., Jassby, D., Gloe, K., Gordon, A. D. & Wiesner, M. R.** (2013) Aquatic biofouling prevention by electrically charged nanocomposite polymer thin film membranes. *Environ. Sci. Technol., 47* (6) pp. 2760–2768.

[34] **Yin, J., Yang, Y., Hu, Z., & Deng, B.** (2013) Attachment of silver nanoparticles (AgNPs) onto thin-film composite (TFC) membranes through covalent bonding to reduce membrane biofouling. *J. Memb. Sci., 441,* 73–82,

[35] **Goh, K., Karahan, H. E., Wei, L., Bae, T. H., Fane, A. G., Wang, R., Chen, Y.** (2016). Carbon nanomaterials for advancing separation membranes: A strategic perspective. *Carbon, 109,* 694–710.

[36] **Hummer, G.** (2007) Water, proton, and ion transport: From nanotubes to proteins," *Mol. Phys., 105* (2-3), 201–207.

[37] **Park, J. H., Sinnott, S. B., & Aluru, N. R.** (2006) Ion separation using a Y-junction carbon nanotube. *Nanotechnology, 17* (3), 895–900.

[38] **Corry, B.** (2007) Designing Carbon Nanotube Membranes for Efficient Water Desalination. *J. Phys. Chem. B, 112* (5), 1427–1434.

[39] **Corry, B.** (2011) Water and ion transport through functionalised carbon nanotubes: Implications for desalination technology. *Energy Environ. Sci., 4* (3), 751–759.

[40] **Thomas, M. and Corry B.** (2016). A computational assessment of the permeability and salt rejection of carbon nanotube membranes and their application to water desalination. *Phil. Trans. R. Soc. A, 374:20150020*.

[41] **Hinds, B. J., Chopra, N., Rantell, T., Andrews, R., Gavalas, V., & Bachas, L. G.** (2004). Aligned Multiwalled Carbon Nanotube Membranes. *Science, 303* (5654), 62–65.

[42] **Majumder, M., Chopra, N., & Hinds, B. J.** (2005) Effect of tip functionalization on transport through vertically oriented carbon nanotube membranes. *J. Am. Chem. Soc., 127* (25), 9062–9070.

[43] **Fornasiero, F., Park, H. G., Holt, J. K., Stadermann, M., Grigoropoulos, C. P., Noy, A., & Bakajin, O.** (2008) Ion exclusion by sub-2-nm carbon nanotube pores. *Proc. Natl. Acad. Sci., 105* (45), 17250–17255.

[44] **Ratto, T. V., Holt, J. K., & Szmodis, A. W.** (2011). *U.S. Patent No. 7993524B2: Membranes with embedded nanotubes for selective permeability*. Washington, DC: U.S. Patent and Trademark Office.

[45] **Zhang L., Shi, G., Qiu, S., Cheng, L., & Chen, H.** (2011). Preparation of high-flux thin film nanocomposite reverse osmosis membranes by incorporating functionalized multi-walled carbon nanotubes. *Desalin. Water Treat., 34* (1-3), 37–41.

[46] **Amini, M., Jahanshahi, M., & Rahimpour, A.** (2013) Synthesis of novel thin film nanocomposite (TFN) forward osmosis membranes using functionalized multi-walled carbon nanotubes,. *J. Memb. Sci., 435*, 233–241.

[47] **Zhao, H., Qiu, S., Wu, L., Zhang, L., Chen, H., & Gao, C.** (2014) Improving the performance of polyamide reverse osmosis membrane by incorporation of modified multi-walled carbon nanotubes. *J. Memb. Sci., 450*, 249–256.

[48] **Lee, H. D., Kim, H. W., Cho, Y. H., & Park, H. B.** (2014) Experimental evidence of rapid water transport through carbon nanotubes embedded in polymeric desalination membranes. *Small, 10* (13), 2653–2660.

[49] **Xue, S. M., Xu, Z. L., Tang, Y. J., & Ji, C. H.** (2016). Polypiperazine-amide

Nanofiltration Membrane Modified by Different Functionalized Multiwalled Carbon Nanotubes (MWCNTs). *ACS Appl. Mater. Interfaces*, *8* (29), 19135–19144.

[50] **Baek, Y., Kim, H. J., Kim, S. H., Lee, J. C., & Yoon, J.** (2017). Evaluation of carbon nanotube-polyamide thin-film nanocomposite reverse osmosis membrane: Surface properties, performance characteristics and fouling behavior. *J. Ind. Eng. Chem.*, *56*, 327–334.

[51] **Al-Hobaib, A. S., Al-Sheetan, K. M., Shaik, M. R., & Al-Suhybani, M. S.** (2017). Modification of thin-film polyamide membrane with multi-walled carbon nanotubes by interfacial polymerization. *Appl. Water Sci.*, *7* (8), 4341–4350.

[52] **Vatanpour, V., Safarpour, M., Khataee, A., Zarrabi, H., Yekavalangi, M. E., & Kavian, M.** (2017). A thin film nanocomposite reverse osmosis membrane containing amine-functionalized carbon nanotubes. *Sep. Purif. Technol.*, *184*, 135–143.

[53] **Wang, J., Yang, D., Gao, X., Wang, X., Li, Q., & Liu, Q.** (2017). Tip and inner walls modification of single-walled carbon nanotubes (3.5 nm diameter) and preparation of polyamide/ modified CNT nanocomposite reverse osmosis membrane. *J. Exp. Nanosci.*, *13* (1), pp. 11–26.

[54] **Zheng, J., Li, M., Yao, Y., Zhang, X., & Wang, L.** (2017) Zwitterionic carbon nanotube assisted thin-film nanocomposite membranes with excellent efficiency for separation of mono/divalent ions from brackish water. *J. Mater. Chem. A*, 5 (26), 13730–13739.

[55] **Kozono, D., Yasui, M., King, L. S., & Agre, P.** (2002). Aquaporin water channels: Atomic structure and molecular dynamics meet clinical medicine. *J. Clin. Invest.*, *109* (11), 1395–1399.

[56] **Wree, D., Wu, B., Zeuthen, T., & Beitz, E.** (2011). Requirement for asparagine in the aquaporin NPA sequence signature motifs for cation exclusion. *FEBS J.*, *278* (5), 740–748.

[57] **Wu, B., Steinbronn, C., Alsterfjord, M., Zeuthen, T., & Beitz, E.** (2009). Concerted action of two cation filters in the aquaporin water channel. *EMBO J.*, *28* (15), 2188–2194.

[58] **Bajaj, P., Mikoryak, C., Wang, R., Bushdiecker, D. K., Draper, R. K., Dieckmann, G. R., Pantano, P., & Musselman, I. H.** (2014). A carbon nanotube-based Raman-imaging immunoassay for evaluating tumor targeting ligands. *Analyst*, *139* (12), 3069–3076.

[59] **Graupner, R.** (2007). Raman spectroscopy of covalently functionalized single-wall carbon nanotubes. *J. Raman Spectrosc.*, *38*, 673–683.

[60] **Irurzun, V. M., Ruiz, M. P., & Resasco, D. E.** (2010). Raman intensity

measurements of single-walled carbon nanotube suspensions as a quantitative technique to assess purity. *Carbon, 48* (10), 2873–2881.

[61] **Attal, S., Thiruvengadathan, R., & Regev, O.** (2006). Determination of the concentration of single-walled carbon nanotubes in aqueous dispersions using UV-visible absorption spectroscopy. *Anal. Chem., 78* (23), 8098–8104.

[62] **Park, C., Wilkinson, J., Banda, S., Ounaies, Z., Wise, K. E., Sauti, G., Lillehei, P. T., & Harrison, J. S.** (2006). Aligned single-wall carbon nanotube polymer composites using an electric field. *J. Polym. Sci. Part B Polym. Phys., 44* (12), 1751–1762.

[63] **Hwang, J., Gommans, H. H., Ugawa, A., Tashiro, H., Haggenmueller, R., Winey, K. I., Fischer, J. E., Tanner, D. B., & Rinzler, A. G.** (2000) Polarized spectroscopy of aligned single-wall carbon nanotubes. *Phys. Rev. B - Condens. Matter Mater. Phys., 62* (20), 310–313.

[64] **Mansfield, E., Kar, A., & Hooker, S. A.,** (2010). Applications of TGA in quality control of SWCNTs. *Anal. Bioanal. Chem., 396* (3), 1071–1077.

[65] **Surapathi, A.** (2012). *Functionalized Single Walled Carbon Nanotube/Polymer Nanocomposite Membranes for Gas Separation and Desalination* (Doctoral dissertation). Virginia Polytechnic Institute, Virginia.

[66] **Kim, Y. S. and Park, C. R.** (2016). Chapter 13 - Titration Method for the Identification of Surface Functional Groups. In M. Inagaki and F. Kang (Eds.), *Materials Science and Engineering of Carbon,* (pp.273-286) Butterworth-Heinemann.

[67] **Chan, W.** (2015). *Functionalized Single Walled Carbon Nanotube / Polyamide Nanocomposite Membranes for Water Desalination* (Doctoral dissertation). Virginia Polytechnic Institute, Virginia.

[68] **Jin, Y. and Su, Z.** (2009). Effects of polymerization conditions on hydrophilic groups in aromatic polyamide thin films. *J. Memb. Sci., 330* (1), 175–179.

[69] **Rao, A. M., Jorio, A., Pimenta, M. A., Dantas, M. S. S, Saito, R., Dresselhaus, G., & Dresselhaus, M. S.** (2000) Polarized Raman Study of Aligned Multiwalled Carbon Nanotubes. *Phys. Rev. Lett., 84* (8), 1820–1823.

CURRICULUM VITAE

Name Surname **:** Aysa Güvensoy

Place and Date of Birth **:** Akhisar, 09.06.1993

E-Mail **:** guvensoy@itu.edu.tr

EDUCATION

- **B.Sc.** **:** 2016, Istanbul Technical University,
  Faculty of Chemical and Metallurgical Engineering,
  Department of Chemical Engineering
- **B.Sc. (Double Major)** **:** 2017, Istanbul Technical University,
  Faculty of Science and Letters,
  Department of Molecular Biology and Genetics
- **M.Sc.** **:** (to date), Istanbul Technical University,
  Grad. School of Science, Engineering and Tech.,
  Chemical Engineering Graduate Program

PROFESSIONAL EXPERIENCE AND REWARDS:

- 2017 – to date : Research Assistant at Istanbul Technical University,
  Department of Chemical Engineering

OTHER PUBLICATIONS, PRESENTATIONS AND PATENTS:

- **Güvensoy, A., Altuntaş, G., Velioğlu, S., Tantekin-Ersolmaz, Ş.-B.** İnce Film Kompozit Desalinasyon Membranı Özeliklerine Destek Tabakası Yapısının Etkisi. 12. Ulusal Kimya Mühendisliği Kongresi, 23-26 Ağustos 2016, İzmir. (Poster presentation).
- **Güvensoy, A., Kürklü, S., Velioğlu, S., Tantekin-Ersolmaz, Ş.-B.** "İnce Film Kompozit Desalinasyon Membranı Özeliklerine Destek Tabakası Yapısının Etkisi", MEMTEK-2017, 5. Ulusal Membran Teknolojileri ve Uygulamaları Sempozyumu, 21-23 Eylül 2017, (Oral presentation).
- **Güvensoy, A., Kürklü, S., Velioğlu, S., Ahunbay, M. G., Tantekin-Ersolmaz, Ş.-B.** "Polyamide/CNT Thin Film Nanocomposite Membranes for Simultaneous Boron Removal and Desalination of Seawater", Euromembrane 2018, Valencia, Spain, July 9-13, 2018. (Poster presentation).